Inhibition of *miR-25* Improves Cardiac Contractility in the Failing Heart

Christine Wahlquist[1,*], **Dongtak Jeong**[2,*], **Agustin Rojas-Muñoz**[1], **Changwon Kho**[2], **Ahyoung Lee**[2], **Shinichi Mitsuyama**[2], **Alain van Mil**[1,3], **Woo Jin Park**[4], **Joost P. G. Sluijter**[3], **Pieter A. F. Doevendans**[3], **Roger J. Hajjar**[2], and **Mark Mercola**[1]

Mark Mercola: mmercola@sanfordburnham.org

[1]Department of Bioengineering, University of California, San Diego, and the Muscle Development and Regeneration Program, Sanford-Burnham Medical Research Institute, 10901 North Torrey Pines Road, La Jolla, California 92037 [2]The Cardiovascular Research Center, Icahn School of Medicine at Mount Sinai, New York, NY 10029 [3]Department of Cardiology, University Medical Center Utrecht, Utrecht, the Netherlands and ICIN, Netherlands Heart Institute, Utrecht, the Netherlands [4]Global Research Laboratory, Gwangju Institute of Science and Technology, Gwangju, Korea

Abstract

Heart failure is characterized by a debilitating decline in cardiac function[1], and recent clinical trial results indicate that improving the contractility of heart muscle cells by boosting intracellular calcium handling might be an effective therapy[2,3]. microRNAs (miRs) are dysregulated with heart failure[4,5] but whether they control contractility or constitute therapeutic targets remain speculative. Using high throughput, functional screening of the human microRNAome, we identified miRs that suppress intracellular calcium handling in heart muscle by interacting with mRNA encoding the sarcoplasmic reticulum calcium uptake pump SERCA2a. Of 875 miRs tested, *miR-25* potently delayed calcium uptake kinetics in cardiomyocytes *in vitro* and was upregulated in heart failure, both in mice and humans. Whereas AAV9-mediated overexpression of *miR-25 in vivo* resulted in a significant loss of contractile function, injection of an antisense oligonucleotide (antagomiR) against *miR-25* dramatically halted established heart failure in a mouse model, improving cardiac function and survival relative to a control antagomiR. These data reveal that increased expression of endogenous *miR-25* contributes to declining cardiac function during heart failure and suggests that it might be targeted therapeutically to restore function.

Keywords

heart failure; microRNAs; miRNAs; sarcoplasmic reticulum; SERCA2a; calcium

Heart failure is the culmination of diverse cardiovascular diseases, including hypertension, ischemic disease and atherosclerosis, valvular insufficiency, myocarditis, or contractile protein mutations, and is uniformly characterized by a progressive loss of contractile function and reserve[1]. The prevailing therapeutic strategy is to block the deleterious effects of the renin-angiotensin and sympathetic systems, but existing drugs target few mechanisms within the failing cardiomyocyte and there is a critical need for novel drugs especially in patients with advanced heart failure[6,7]. A complex intracellular network balances contractility and intracellular Ca^{2+} handling in relationship to workload[8]; however, the role of miRs in cardiac contractility remains largely unexplored. miRs fine-tune nearly all normal and pathological processes examined by downregulating proteins that occupy key nodal points in biological control networks[9,10]. We reasoned that miRs that repress contractility[11] might be upregulated during human heart failure, and might therefore constitute novel targets for therapeutic intervention.

The calcium-transporting ATPase SERCA2a, also known as ATP2A2, is the primary mechanism for Ca^{2+} uptake during excitation–contraction coupling in cardiomyocytes. Impaired Ca^{2+} uptake resulting from decreased expression and reduced activity of SERCA2a is a hallmark of heart failure[2]. Accordingly, restoration of SERCA2a by gene transfer has proven effective in improving key parameters of heart failure in animal models[12] and more recently in clinical trials[13]. Thus, miRs that downregulate SERCA2a might be elevated in heart failure and compromise cardiac function. Computational algorithms predict >300 miRs target SERCA2a (miRNA Data Integration Portal[14]), but are error-prone necessitating empirical evaluation[15]. We therefore functionally screened a whole-genome collection of miRs for selective downregulation of the Ca^{2+} pump. To perform the screen, we fused the SERCA2a mRNA 3'UTR sequence downstream of an eGFP coding region, making a "target sensor" construct to permit detection of active miRs by a decrease of eGFP fluorescence (Fig. 1a,b). In the primary screen, 144 miRs reduced eGFP fluorescence by >30% with $P<0.05$ (Fig. 1c,d), and 82 were confirmed by testing through a dose range (Fig. 1e,f, Supplementary Table 1). 32 were evolutionarily conserved and 15 were both evolutionarily conserved and reported to be upregulated in human heart failure (see **Detailed Methods**) (Fig. 1e). 4 caused a highly significant ($P<0.001$, one-tailed ANOVA) prolongation of the decay phase of the Ca^{2+} transient in the cardiomyocyte HL-1 cell line, shown here as duration from 75% to 25% maximal value, $CaTD_{75-25}$ (Fig. 1g), measured using an automated platform[16]. The most potent was *miR-25*, which elicited a physiological effect comparable to that of siSERCA2a (Fig. 1h). We confirmed that *miR-25* is upregulated in human myocardial samples from patients with severe heart failure (Fig. 1i). *In situ* hybridization revealed that *miR-25* is expressed primarily in cardiomyocytes of TAC-induced failing mouse hearts, with no detectable expression in cardiac fibroblasts or vascular endothelial cells, and low expression in vascular smooth muscle (Fig. 2).

To establish a link between *miR-25* and cardiac function, we identified putative protein targets involved in Ca^{2+} handling computationally (DianaLab miRPath with TargetScan Mouse v5.0, see Methods). In addition to SERCA2a, these included inositol-3'-phosphate receptor-1 (IP3R1) that was selectively downregulated by *miR-25* transient transfection in HL-1 cells (Fig. 3a, Extended Data Fig. 1a). Other candidate proteins involved in calcium handling, including the sodium-calcium exchanger (NCX1), calmodulin kinase-2 (CaMKII), phospholamban (PLN) and Calmodulin-3 (Calm3) were unaffected in HL-1 cells transfected with *miR-25* (Extended Data Fig. 2). miRs bind cognate mRNAs by imprecise base pairing to specific recognition elements[9,10]. Single putative *miR-25* recognition sites were identified within SERCA2a and IP3R1 3'UTR sequences by TargetScan Human v6.2 (Fig. 3b, Extended Data Fig. 1b). Mutation of these sequences abolished the ability of *miR-25* to inhibit reporter expression (Fig. 3b, Extended Data Fig. 1b), further supporting selective *miR-25* interactions with the mRNAs, and indicating that the single recognition elements identified in the 3'UTRs of the SERCA2a and IP3R1 are sufficient for *miR-25* activity.

Having shown that *miR-25* regulates SERCA2a and IP3R1, we evaluated whether siRNAs directed against these proteins could mimic the effect of *miR-25* on cardiac Ca^{2+} transient kinetics *in vitro*. Transfection of siRNA against SERCA2a significantly slowed the decay (Ca^{2+} re-uptake) phase of the transient ($CaTD_{75-25}$) relative to controls in spontaneously contracting HL-1 cells (Fig. 3c, Extended Data Fig. 1c) and neonatal rat ventricular cardiomyocytes (NRVCs, Extended Data Fig. 1d); however, the upstroke V_{max} was unchanged (Extended Data Fig. 3), accurately reproducing the effect of *miR-25* and mimicking the ~1.5-2x decline reported for ventricular cardiomyocytes isolated from failing human hearts[17,18]. siRNA against IP3R1 only minimally affected Ca^{2+} transient kinetics in HL-1 cells and not at all in NRVCs ($CaTD_{50}$, $CaTD_{75-25}$, and Ca^{2+} transient upstroke V_{max}, (Fig. 3c, Extended Data Fig. 3), suggesting that the predominant effect of *miR-25* on Ca^{2+} transient kinetics is mediated through downregulation of SERCA2a.

We evaluated the physiological effect of blocking *miR-25*. AntagomiRs are antisense oligonucleotides modified to enhance duplex stability and have been used effectively to inhibit miR function *in vitro* and *in vivo*[19]. Anti-*miR-25* transfection alone decreased the Ca^{2+} transient duration (decreased $CaTD_{75-25}$) in HL-1 cells but had no effect in NRVCs (Fig. 3c, Extended Data Fig. 1d). Importantly, when co-transfected, the anti-*miR-25* cancelled the prolonging effect of *miR-25* on $CaTD_{75-25}$, restoring kinetic parameters to near normal in both cell types.

We next assessed the physiological consequences of administering *miR-25* and anti-*miR-25* *in vivo.* AAV9-mediated gene transfer of *miR-25* increased the levels of *miR-25* by approximately 50% and correspondingly decreased SERCA2a levels in ventricular myocardium (Fig. 3d–f), causing a progressive decline in fractional shortening (%FS), an index of cardiac function (Fig. 3g,h). Hemodynamic analyses at the termination of the studies (6 weeks after AAV transfer) confirmed that LV function had declined in *miR-25*-injected mice (Fig. 3i–k and Extended Data Fig. 4b,c). In contrast, AAV-transfer of *miR-92a* (Fig. 3d,e), which has the same seed sequence (AUUGCAC) as *miR-25*, did not affect SERCA2a levels (Fig. 3f) nor significantly affect LV function (Fig. 3g–k; Extended Data Fig. 4b,c), although it downregulated integrin α5, a target involved in angiogenesis[20]

(Extended Data Fig. 4a) despite identical copy number of integrated AAV genomes (Extended Data Fig. 5). Together, these results point to a selective interaction between *miR-25* and SERCA2a mRNA that is consistent with the importance of non-seed sequences for target specificity[21], and also indicate that elevated *miR-25* can depress cardiac function. Evaluating selectivity and efficacy of anti-*miR-25*, we intravenously injected anti-miRs formulated with *in vivo*-jetPEI™ reagent mixture. Anti-*miR-25* injection decreased endogenous *miR-25* levels in LV myocardium of both WT and SERCA2a KO mice relative to treatment with a control (scrambled sequence) anti-miR (Extended Data Fig. 6a), but did not affect *miR-92a* (Extended Data Fig. 7). Accordingly, anti-*miR-25* increased SERCA2a levels as expected in WT mice (Extended Data Fig. 6b). Notably, however, anti-*miR-25* did not improve the cardiac morphometric or hemodynamic parameters of SERCA2a knockout mice (Extended Data Fig. 8), suggesting that the Ca^{2+} pump is a critical target for *miR-25*.

Since *miR-25* decreased SERCA2a levels *in vitro* and *in vivo*, we evaluated whether administration of anti-*miR-25* would affect cardiac function during chronic heart failure. Mice were subjected to 3 months of TAC to chronically increase LV load and cause LV dilation prior to administering anti-*miR-25*. Once heart failure was established, anti-*miR-25* or control anti-miR were injected intravenously and subsequently monitored for effects on heart function (Fig. 4a). Echocardiography revealed substantial improvements in cardiac function following injection of anti-*miR-25* at 4.5 and 5.5 months after TAC, despite constant pressure overload, compared with severe deterioration in animals injected with the control anti-miR (Fig. 4b,c and Supplementary Table 2). Furthermore, hemodynamic analyses at the termination of the studies (5.5 months post-TAC) showed substantially improved LV function in the anti-*miR-25*-injected mice, effectively restoring the load-independent parameter end systolic pressure volume relationship (ESPVR) and EF to normal levels (Fig. 4d–f and Supplementary Table 3). The heart-weight to body-weight ratio was also stabilized (Fig. 4g). Survival of the TAC-induced heart failure animals was also improved; with 7/8 anti-*miR-25*-injected and 8/8 sham-operated animals surviving versus 7/22 of the control anti-miR-injected animals (Kaplan Meier analysis, Extended Data Fig. 9), reflected by an increased probability of survival of TAC animals injected with anti-*miR-25* versus control anti-miR *(P* = 0.0131, Log-rank test). Consistent with improved cardiac function, anti-*miR-25*-injected mice had significantly reduced levels of endogenous *miR-25* compared to control animals (both TAC (Fig. 4h) and sham-operated (Extended Data Fig. 6a). Neither anti-*miR-25* nor the control anti-miR affected the cardiac physiology of sham-operated animals (Extended Data Fig. 8). Total and SUMOylated SERCA2a levels were significantly increased (Fig. 4i and Extended Data Fig. 10), indicating that anti-*miR-25* injection restored the loss of SERCA2a protein as well as post-translational modifications of SERCA2a such as SUMOylation (that improves transporter stability and ATPase activity[22]) despite the prior onset of heart failure. Furthermore, injection of anti-*miR-25* reduced fibrosis (Fig. 4j–l, n–p, r–t, v) and also normalized cardiomyocyte cell size (Fig. 4m,q,u,w). Given that the anti-*miR-25* had no salutary effect on cardiac morphometric or hemodynamic parameters in SERCA2a knockout mice (Extended Data Fig. 8), did not affect expression of other miRs with homologous seed sequences (Extended Data Fig. 7), and that AAV9-cardiac transfer of *miR-25* selectively affected SERCA2a (Fig. 3f), we propose that the beneficial effect of anti-*miR-25* is due to inhibition of pathologically upregulated

endogenous *miR-25* and subsequent restoration of SERCA2a activity. To our knowledge, these data provide the first evidence that cardiac delivery of an anti-miR can directly control SERCA2a protein levels in order to achieve long-term improvement of cardiac function.

These studies identified *miR-25* as a critical repressor of SERCA2a and cardiac function during heart failure. Of note, several mechanisms beyond SERCA2a deficiency, such as changes in K^+ channel density, NCX expression and myofilament sensitivity to Ca^{2+}, also contribute to slowing of the Ca^{2+} transient in advanced heart failure[23]. *miR-25* might also control IP3R1, and thus could be involved under conditions of IP3 sensitization, such as in response to endothelin-1, angiotensin and phenylephrine[24] or in local Ca^{2+} control[25]. The NAD(P)H oxidase-4 (NOX4) was recently shown to be downregulated by *miR-25* in a mouse model of diabetic nephropathy[26]; however, NOX4 levels did not change significantly in our long-term TAC heart failure model (not shown). Whether NOX4, which is responsible for the production of superoxide, might contribute to the salutary effects of anti-*miR-25* therapy is unclear since it is reported to confer both protective and detrimental effects[27]. Finally, *miR-25* was recently reported to decrease acutely after aortic constriction in mice[28], in contrast to the chronic elevation reported here and in human heart failure samples, perhaps reflecting the very different stages of pathogenesis. In conclusion, our data suggest that inhibition of *miR-25* may be a novel therapeutic strategy for the treatment of heart failure.

Methods Summary

Detailed Methods are available with the online version of this paper.

For primary screening, HEK293 cells were co-transfected with the Ambion® Pre-miR™ miRNA Precursor Human V2.0 microRNA library (25nM) and 300 ng Serca2a 3'UTR target sensor plasmid (Fig. 1a) per well in 384-well plates, in triplicate.

For secondary screening, Ca^{2+} transient recordings (10 seconds, 33 frames per second) were acquired from HL-1 and NRVCs transfected with candidate miRs and loaded with Hoechst 33342 and Fluo-4 72 hours post-transfection, and analyzed to derive cytoplasmic calcium transient kinetic parameters using KIC instrument and software (Vala Sciences). Unresponsive or low responding cells were removed by gating. Statistical significance was determined using one-way ANOVA.

All mice were housed and treated in accordance with guidelines from the NIH and institutional animal care and use committees, and protocols were approved by the Mount Sinai School of Medicine or SBMRI animal care and use committees.

Left ventricular samples were from explanted hearts of patients with severe heart failure samples at the time of cardiac transplantation. Non-failing hearts (controls) were from patients who died of cerebrovascular accidents with no evidence of contractile dysfunction by echocardiography. The 5 non-failing hearts (3 males and 2 females) had a median age of 43. The 5 heart-failure patients (4 males and 1 female) had a median age of 54 and their mean ejection fraction prior to cardiac transplantation was $22\pm3\%$.

MATERIAL TO BE INCLUDED WITH THE ONLINE VERSION

Methods

Cell culture—HEK293 cells were maintained in DMEM/F12 supplemented with 10% FBS, 100 units/ml penicillin and 100 μg/ml streptomycin. HL-1 cells were maintained in Claycomb Medium (Sigma) supplemented with 10% FBS (Sigma), 100 units/ml penicillin, 100 ug/ml streptomycin, 2mM L-glutamine, 0.1mM norepinephrine (Sigma) and passaged approximately every 3–4 days when cells reached confluency and spontaneous contractions were observed. For transient transfection of both cell lines, Lipofectamine 2000 (Life Technologies) was used following manufacturer's protocol. Cy3 labeled negative control siRNA (Ambion, AM4621) or microRNA (Ambion, AM17120) was used for control in all transfection experiments. Transfection efficiency was >90%.

Neonatal rat ventricular cardiomyocytes (NRVCs) were isolated with the neonatal rat cardiomyocyte isolation kit (Worthington) and cultured at 37°C with 5% CO2. In brief, ventricles were dissected from 1–2-d-old Hsd:SD rats (Sprague Dawley), then digested overnight at 4°C with trypsin. Digestion continued the following morning with collagenase for approximately 90 minutes at 37°C. Cells were pooled, pre-plated for 90 min on an uncoated dish to remove fibroblasts, and transfected as above on matrigel-coated cell culture plastic dishes in high-serum media (DMEM/F12 [1:1], 0.2% BSA, 3 mM sodium-pyruvate, 0.1 mM ascorbic acid, 4 mg/liter transferrin, 2 mM L-glutamine, 100 nM thyroid hormone (T3) supplemented with 10% horse serum and 5% FCS) at 2×10^5 cells/cm^2. After 24 h, media was changed to low-serum medium (same but with 0.25% FCS). At 72 h cells were processed for calcium imaging (see below).

Target sensor—To screen for microRNA repression of the cardiac-specific *Serca2a* isoform we substituted the CMV promoter of the pDsRed-N1 vector (Clontech) with the hPGK promoter driving expression of eGFP. We focused on the *Serca2a* 3'UTR since it is selectively expressed in cardiomyocytes (in contrast to *Serca2b* sequences) to test the hypothesis that the cardiac-specific isoform might be under distinct regulatory control. DsRed sequence was replaced with the human *Serca2a* 3' UTR sequence (nucleotides 3503-4302, Genbank accession number NM_001681.3), which was obtained by PCR of differentiated human ES cells displaying spontaneous contractions. Primer sequences used for amplification were as follows:

hSerca2a F: 5'-CGGGGTACCTGCAATACTGGAGTAACCGCTTC -3'

hSerca2a R: 5'- CGGCGGCCGCATTTACCTGAAACCATGTCTGTGC -3'

microRNA Screen—HEK293 cells were co-transfected with the Ambion® Pre-miR™ miRNA Precursor Human V2.0 microRNA library and 300 ng Serca2a 3'UTR target sensor plasmid per well in 384-well plates (Greiner). Transfections were performed using Lipofectamine 2000 (Life Technologies) in triplicate with 25nM of each miR. At 48 h after transfection cells were fixed in 4% paraformaldehyde and imaging was performed using an automated fluorescent microscope (InCell Analyzer 1000; GE Healthcare) and analyzed using CyteSeer software (Vala Sciences) by quantifying Total Integrated Pixel Intensity within an eGFP-positive area, as described[29,30]. Hits were confirmed by a 5-point dose

response assay (50nM to 3.125nM), and data plotted (Fig. 1e) as area under curve (A.U.C.). 32 were determined to be evolutionarily conserved between mouse and human (TargetScan v6.2), and 15 were both evolutionarily conserved and reported to be upregulated in human heart failure[4,5,31–37].

Site-directed mutagenesis—Site-directed mutagenesis was used to modify the *miR-25* seed binding sequence using *Pfu Turbo* DNA Polymerase. *Dpn* I was used to digest non-mutated DNA template before transforming the mutated plasmids. Primers used were as follows:

Serca2a 3'UTR F: 5'- GCAGTAGACAGATGTTG**TTCGAA**TACAAATATTGTGATGC -3'

Serca2a 3'UTR R: 5'- GCATCACAATATTTGTA**TTCGAA**CAACATGTGTCTACTGC -3'

IP3R1 3'UTR F: 5'- ATGTTTTTTATAAAACT**CATATG**TACGAATTATGCAATCAC -3'

IP3R1 3'UTR R: 5'- GTGATTGCATAATTCGTA**CATATG**AGTTTTATAAAAAACAT -3'

The mutated sequences were designed to contain restriction enzyme recognition sites (marked in bold) used to verify correct mutation of the seed site.

IP3R1 Target sensor luciferase assay—HEK293 cells were co-transfected with microRNA (25nM) and 100 ng human IP3R Type 1 miTarget (GeneCopoeia). 48 h after transfection reporter activity was analyzed using the Dual-Glo® Luciferase Assay System (Promega) and EnVision plate reader (PerkinElmer). Data are presented as a ratio of firefly luciferase activity normalized to Renilla luciferase.

Quantitative RT-PCR—RNA was isolated from human tissue using Trizol (Life Technologies) according to manufacturer's protocol. All-in-One™ miRNA qRT-PCR Detection Kit (GeneCopoeia) was used for both cDNA synthesis and quantitative detection using *miR-25* specific primers (GeneCopoeia). *Rnu6* was used for normalization.

RNA was isolated from mouse tissue using mirVana™ miRNA Isolation kit (Life Technologies) according to manufacturer's protocol. The TaqMan® MicroRNA Assays kit (Life Technologies) was used for both cDNA synthesis and quantitative PCR using *miR-25* primers (Life Technologies). *miR-24* was used for normalization.

***In Situ* hybridization—**To characterize the distribution and cellular origin of *miR-25* in heart failure we performed *in situ* hybridization on 10 μm thick cryosections of TAC-induced heart failure mice (1 month post-TAC). Sections were fixed by 4% paraformaldehyde for 10 minutes, acetylated for 10 minutes and permeabilized for 5 minutes by proteinase K treatment (5 μg/ml). Prehybridization of sections was performed for four hours at RNA melting temperature (*T*m) minus 30°C (specific for each LNA probe) before overnight hybridization with 25 nM 5`-DIG and 3`-DIG labeled miRCURY LNA

microRNA detection probes (Exiqon) for *miR-25* (18122-15), negative control *miR-159* (99003-15), and positive control U6 (99002-15) at *T*m minus 30°C in denaturing hybridization buffer. To remove unbound and partially bound probes slides were washed for 15 minutes in 5X SSC and 1 hour in 0.2X SSC at 60°C. After washing, sections were blocked for 1 hour before overnight incubation at 4°C with anti-DIG-alkaline phosphatase antibody (1:1500, Roche). For miRNA visualization sections were subsequently incubated in Liquid Permanent Red (Dako) for 6 hours. Co-staining for the non-cardiomyocyte fraction was performed by incubation with lectin BS-I (1:100, Sigma), anti-α-Smooth Muscle Actin (1:400, Sigma), or Periostin (1:50, Sigma) for 1 hour at room temperature, followed by 1 hour incubation with appropriate Alexa Fluor® 488 secondary antibodies (Life Technologies). Hoechst 33342 (Life Technologies) was used as a counter stain and slides were mounted in Fluoromount G (SouthernBiotech). Images were captured using cellP software (Olympus) on an Olympus BX60 microscope and processed with Adobe Photoshop Cs4 v11.

Protein expression analyses—For *in vitro* transfection experiments using HL-1 cells, cells were transfected with miRs (50nM), and samples were lysed 72 h later using Novex Tris-Glycine 2x Sample Buffer supplemented with 5% β-mercaptoethanol at 55°C for 1 h. Samples were loaded on SDS-polyacrylamide electrophoresis gels for separation, followed by blotting of protein onto polyvinylidene fluoride membrane. Membranes were then incubated as follows: Serca2a (1:2000; 21st Century Biochemicals), IP3R1 (1:200, goat polyclonal, sc-6093; Santa Cruz Biotechnology), Calmodulin (1:2000, rabbit monoclonal, ab45689; Abcam), NCX1 (1:500, mouse monoclonal, MAB1590; Chemicon), GAPDH (1:1000, rabbit polyclonoal, ab9485; Abcam), Phosopholamban (1:500, mouse monoclonal, 05-205; Upstate) and CaMKII (1:10,000, kind gift from Dr. Joan Heller Brown laboratory). Alexafluor-labeled secondary antibodies were used (1:10,000) for detection of the specific bands. Quantitative analysis was done using the Odyssey® imaging system (LI-COR Biosciences).

Calcium imaging and analysis—HL-1 cells were seeded at a density of 25,000 cells/well on 96-well glass bottom plates (Greiner) and transfected with 50nM miRs as described for cell culture above. NRVCs were seeded at a density of 60,000 cells/well, and were processed identically, with the addition of a single 15 V electrical pulse of 5 ms at 1 Hz, initiated at 2 s into recording.

72 h post-transfection, cells were loaded with 200 ng/ml Hoechst 33342 (Sigma) and Fluo-4 for 30 minutes at 37°C followed by 30 minutes at room temperature. Fluo-4 NW Calcium Assay Kit (Life Technologies) was prepared according to manufacturers' instructions in 1x Hanks Balanced Salt Solution containing 20mM HEPES buffer (Life Technologies) and 2.5mM Probenecid (Life Technologies). Following loading, cells were incubated with Tyrode's solution (140mM NaCl, 6mM KCl, 1mM $MgCl_2$, 5mM HEPES, 2mM $CaCl_2$, 10mM glucose, pH 7.4) for imaging. Ca^{2+} transient recordings were done using a Kinetic Image Cytometer IC 100 (Vala Sciences). Video streams of 10 seconds of the Fluo-4 green channel were collected for each well at 33 frames per second. Autofocus by the IC 100 was performed automatically by video acquisition using the nuclear channel. All image capture

was performed with a 20x 0.50 numerical aperture (NA) objective. Cytometric calcium kinetic parameters were determined by image analysis using CyteSeer software (Vala Sciences) and unresponsive or low responding cells were removed by gating.

Bioinformatics—Predicted *miR-25* target binding sites were obtained from TargetScan Human v6.2 (http://www.targetscan.org). Potential targets of *miR-25* involved in calcium signaling pathways were identified using DianaLab miRPath with TargetScan Mouse v5.0 prediction software (http://diana.cslab.ece.ntua.gr/pathways).

AAV9 transduction—AAV9-*miR25* and *92a* were produced using the two-plasmids protocol described by Zolotukhin et al[38] with the following modifications: 293-T cells (ATCC) were grown in triple flasks for 24 hours (DMEM, 10% FBS) prior to the transfection using PEI (polyethyleneimine). After 72 hours, Cells were harvested and only DNase resistant virus was purified by an iodixanol density gradient (Optiprep, Greiner Bio-One Inc). Finally viruses were concentrated and formulated into lactated Ringer's solution (Baxter Healthcare Corporation) using a Vivaspin 20 Centrifugal concentrators 100K MWCO (Vivascience Inc), and stored at – 80°C. On the day of the injection, mice were immobilized using the single mouse restrainer (Harvard apparatus) and indicated amount (5×10^{11} vector genomes (vg) / mouse) of AAV9 was injected through tail-vein.

AAV transduction of *miR-25* and *miR-92a* yielded comparable copy number (Extended Data Fig. 5). To quantify *miR-25 and miR-92a* copy number in mice, we used a SYBR green-based real-time quantitative assay. Genomic AAV9-*miR-25* and *miR-92a* vector DNA was extracted from frozen cardiac tissues by using DNeasy Tissue Kits (Qiagen). The real-time quantitative PCR assay detects a 145-bp sequence unique to SV40 promoter in AAV9 vector (F: TTGGACAAACCACAACTAGAA, R: AACCTCCCACACCTCCC). Genomic DNA was isolated from the indicated tissues and 100 ng of each sample was used in duplicate to determine vector genome copies. The plasmid DNA was used as a copy number standard ranging from 10 to 10^8 copies/μl. The lower limit detection of the assay was 150 copies/μg DNA.

TAC (Trans aortic constriction) surgery—Male mice (B6C3F1 strain) of 8 to 10 weeks of age (25–30 g) were used. The animals were anesthetized with ketamine (95mg/kg) / xylazine (5mg/kg) administered via intraperitoneal injection. The mice were ventilated with a tidal volume of 0.1 ml and a respiratory rate of 110 breaths per minute (Harvard Apparatus). A longitudinal incision of 2 to 3 mm was made in the proximal sternum to allow visualization of the aortic arch. The transverse aortic arch was ligated between the innominate and left common carotid arteries with an overlaid 27-gauge needle. The needle was then immediately removed, leaving a discrete region of constriction. Echocardiography was performed and Doppler was used to calculate the pressure gradient between proximal and distal sites of the transverse aortic constriction. Only animals with a pressure gradient > 30 mmHg were included in this study. After 8 weeks, additional echocardiography was performed to evaluate cardiac function. Only animals with FS < 50% were determined as HF for further study.

Anti-miR administration—Anti-*miR-25* (product ID: AM10584), anti-miR negative control (product ID: AM17010) were purchased from Ambion (Austin, TX). Separate solutions of anti-*miR-25*, anti-miR negative control were each diluted with *in vivo*-jetPEI solution (Cat. No. 201-50, Polyplus-transfection, Illkirch, France) containing 10% (wt/vol) glucose (Polyplus-transfection reagent) at an N/P ratio of 5, following the recommendations of the manufacturer (PolyPlus Transfection) to final doses of oligonucleotide of 300 μg. All solutions were mixed by vortexing for 10 s and incubated for at least 15 min at 37°C prior to injection. Each mouse received 400μl saline and oligonucleotide mixture (100μl of oligonucleotide solution + 300μl of saline) through tail vein injection consecutively for 3 days and 3 additional injections were performed once a week for following 3 weeks. Two additional groups of control animals were included; one consisting of untreated animals and the other of animals receiving a mixture of in vivo jetPEI solution containing 10% (wt/vol) glucose without added oligonucleotide. All injections were carried out using 30G needle syringe with single mouse restrainer (Harvard apparatus, Boston).

Production of SERCA2a Knock-out mice—Conditional SERCA2 KO mice were generously donated by Dr. Geir Christensen, University of Oslo, Norway[39]. The mice were generated by standard gene targeting strategies to introduce loxP sites into introns 1 and 3 of the *Serca2* (*Atpa2a2*) gene. For our studies, 8–10 week-old mice were injected intraperitoneally with 4-OH-tamoxifen (1 mg/day) for 4 days to induce cardiomyocyte-specific excision of the *Serca2* gene sequences, essentially as described [39,40].

Echocardiography and in vivo hemodynamics—B6C3F1 mice were acquired from Jackson laboratories. Mice were anesthetized with intraperitoneal ketamine (100 μg/g) for echocardiographic analysis. Two-dimensional images and M-mode tracings were recorded on the short-axis at the level of the papillary muscle to determine percent fractional shortening and ventricular dimensions (GE Vivid Vision). One day after echocardiography, *in vivo* hemodynamics was performed using a 1.2Fr pressure-volume (PV) conductance catheter (Scisense, Ontario, Canada). Mice were anesthetized with an intraperitoneal injection mixture of urethane (1 mg/g), etomidate (10 μg/g), and morphine (1 μg/g) and were then intubated via a tracheotomy and mechanically ventilated at 7 μl/g tidal volume and 120 respirations/min. The PV catheter was placed in the left ventricle via an apical stab approach as previously described[41]. Pressure-volume data were analyzed using IOX2 software (EMKA technologies). All procedures were approved by and performed in accordance with the Institutional Animal Care and Use Committee of the Mount Sinai School of Medicine. The investigation conforms with the Guide for the Care and Use of Laboratory Animals published by the US National Institutes of Health (NIH Publication No. 85–23, revised 1996).

Histological examination of cardiac tissues—To measure cardiomyocyte cross sectional area, suitable cross-sections with nearly circular capillary profiles and nuclei were selected on sections stained with wheat germ agglutinin (WGA) followed by a FITC-conjugated rabbit polyclonal to WGA (1:100; ab20528, Abcam). These were observed using an Axiophot microscope (Carl Zeiss, Germany), and then analyzed using the Analysis-SIS3.2 software (Soft-Imaging System, Germany). To measure the fibrotic areas, Masson-

trichrome staining kit (Sigma-Aldrich (HT15-1kt), USA) was used for staining of the sectioned hearts. The fibrotic areas stained blue and the normal tissue stained red. The fibrotic area was calculated as the ratio of the total area of fibrosis to the total area of the section.

Statistical analysis—Data are presented as mean ± standard error of the mean (s.e.m.). Unpaired Student's t-test or ANOVA was performed as indicated to determine statistical differences. Whisker box plots show outliers beyond the 5th and 95th percentiles. All statistical analyses were done using GraphPad Prism software.

Extended Data
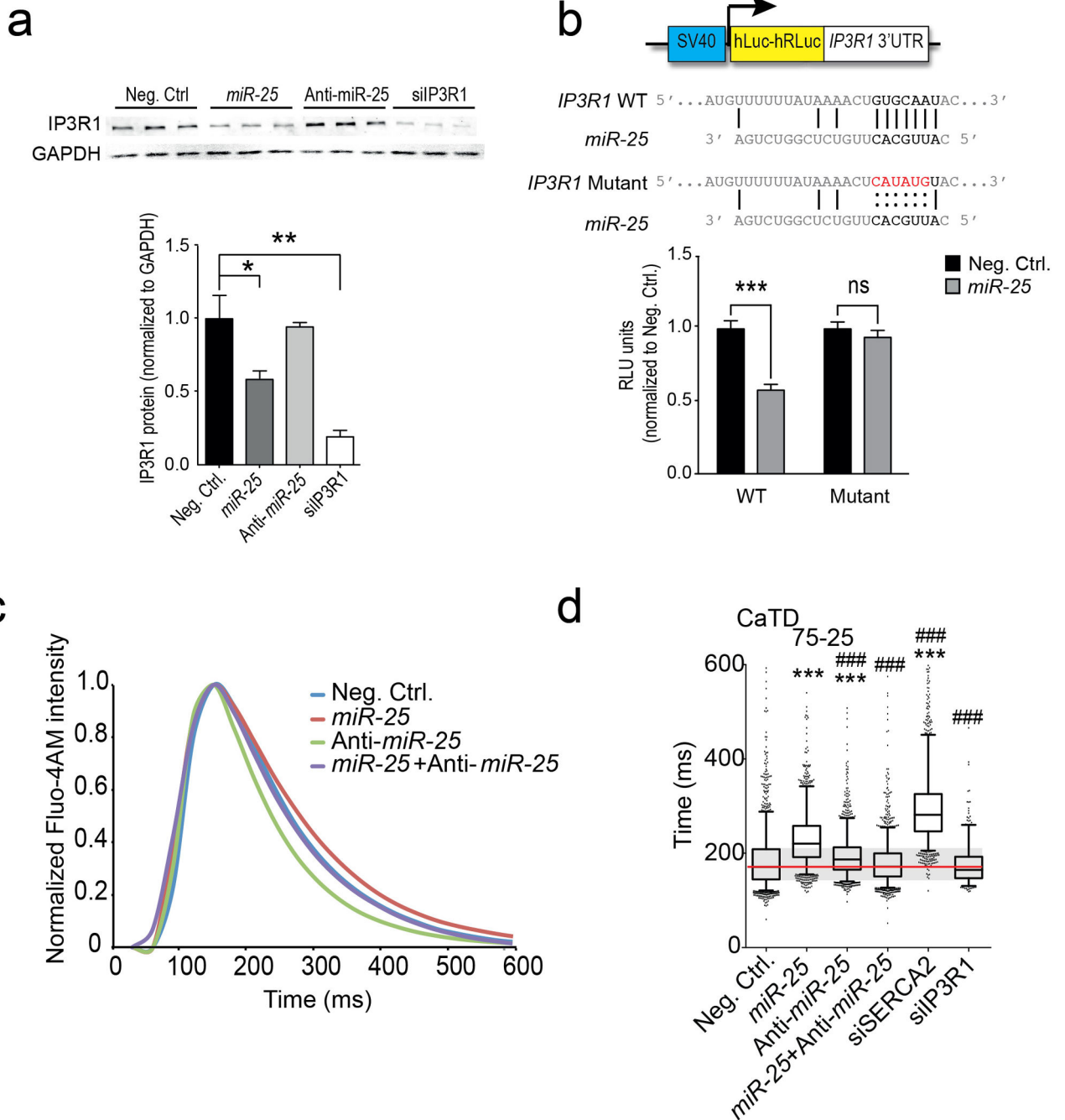
Extended Data Fig. 1. Effect of *miR-25* on IP3R1 and cardiomyocyte calcium transients *in vitro*
Effect of *miR-25*, anti-*miR-25* and siIP3R1 transfection on IP3R1 protein levels in HL-1 cells (**a**). Sequence of the putative *miR-25* target recognition element in IP3R1 mRNA and the corresponding alteration by site-directed mutagenesis (**b**). Mutation abolished inhibition of luciferase signal by *miR-25* (*n*=10). Representative Ca^{2+} transient of HL-1 cells transfected as indicated (**c**). Note that *miR-25* slowed the repolarization phase kinetics,

whereas anti-*miR-25* quickened the kinetics. Co-transfection normalized kinetics. Kinetic imaging cytometry analysis of Ca^{2+} transient kinetics during the decay phase (Ca^{2+} transient duration time from 75% to 25% maximal value, $CaTD_{75-25}$) of transfected NRVC (**d**) (*n*>550 cells). In panels **a,b** data is represented as mean ± s.e.m. In panel **d**, box defines interquartile range; whiskers = ±5th and 95th percentile; dots = outliers
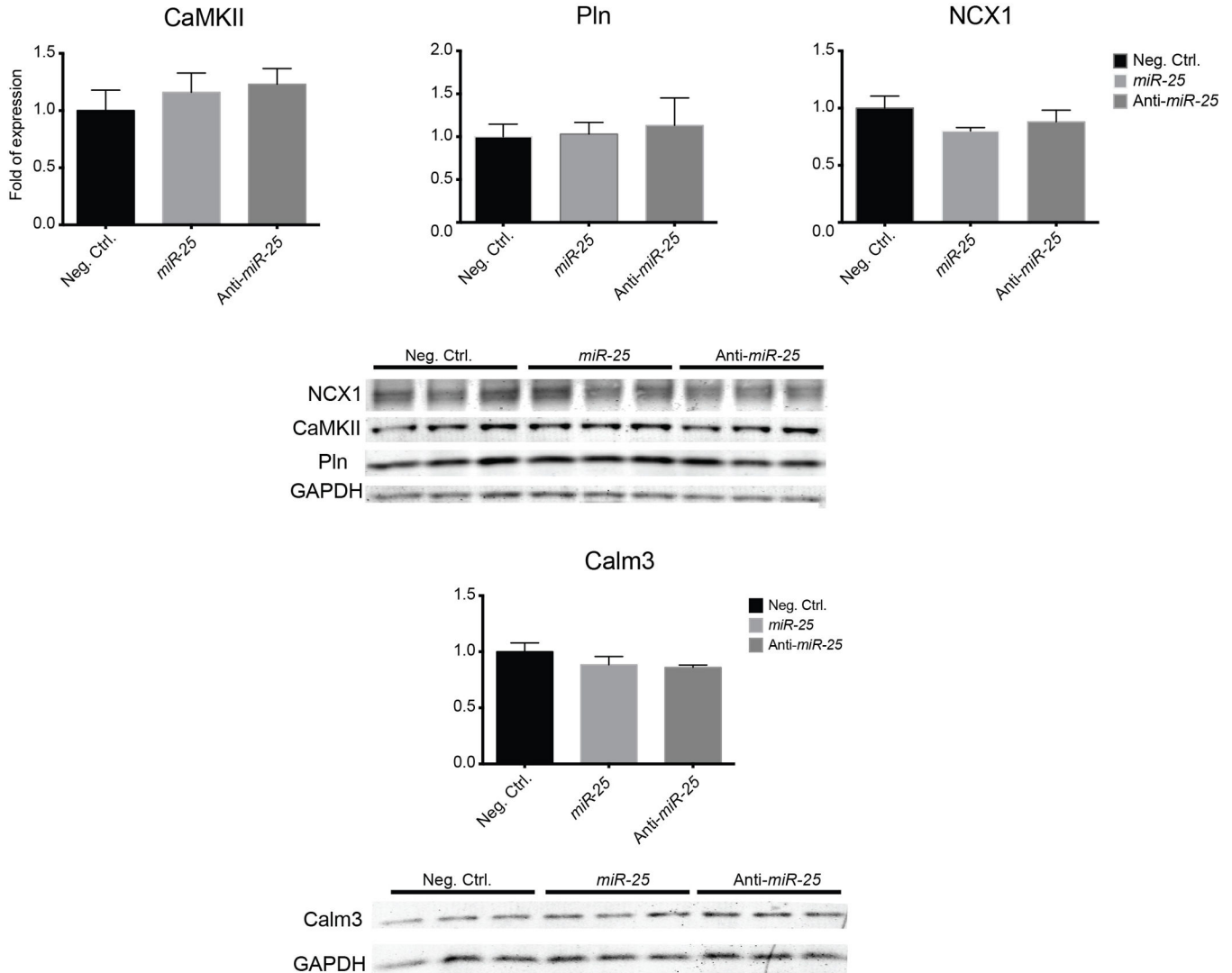
Extended Data Fig. 2. Effect of *miR-25* on calcium handling proteins
Expression of candidate targets of *miR-25* in transfected HL-1 cells (lysates collected 5 days post-transfection). No effect of *miR-25* or *anti-miR-25* was noted for these proteins. Data represented as mean ± s.e.m.
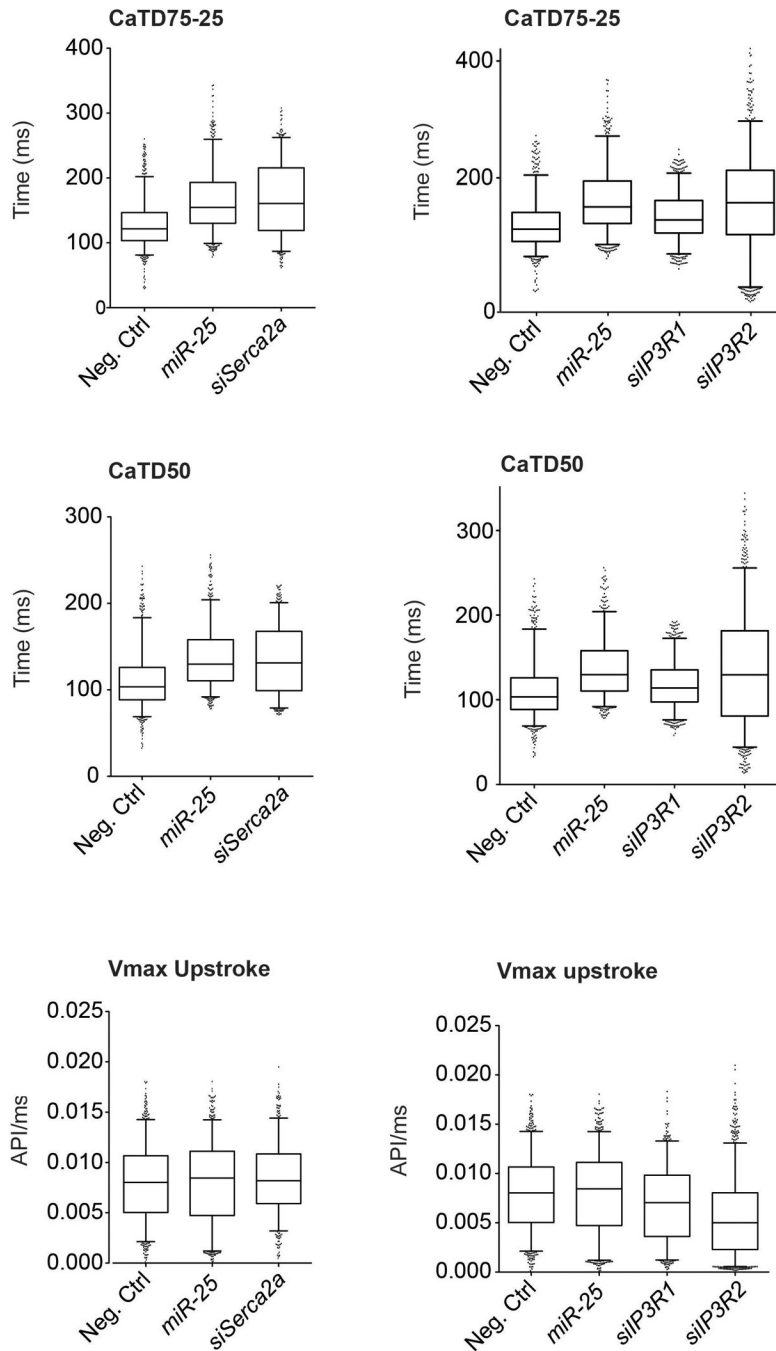
Extended Data Fig. 3. Calcium transient effects of *miR-25* compared to that of siRNAs against SERCA2a and IP3R isoforms

Cardiomyocyte-like HL-1 cells were transfected with *miR-25*, siRNA to SERCA2a (siSERCA2a) (left panels) or siRNAs to IP3R1 or IP3R2 (siIP3R1, siIP3R2) (right panels), and analyzed 72 hours later by kinetic imaging cytometry. Kinetic parameters are CaTD$_{50}$ (Ca^{2+} transient duration 50, which is the time from maximal value to 50% maximal value), CaTD$_{75-25}$ (Ca^{2+} transient duration 75-25, which is the time from 75% maximal value to 25% maximal value), and V$_{max}$ upstroke (the maximal velocity of the upstroke phase of the Ca^{2+} transient). Data are represented as whisker plots, with the box denoting the 25th and

75th percentiles, the whiskers the 5th and 95th percentiles, the middle bar is the median, and outliers are indicated as individual dots.

Note that siSERCA2a and *miR-25* elicited comparable effects, both markedly delaying the Ca^{2+} uptake phase parameters $CaTD_{50}$ and $CaTD_{75-25}$ without appreciably altering V_{max} upstroke kinetics. (*n*>550 cells per group). Box defines interquartile range; whiskers = ±5th and 95th percentile; dots = outliers.

Also note that siIP3R1 only minimally affected the Ca^{2+} kinetic parameters. siIP3R2 slowed V_{max} upstroke and broadened the distribution of uptake phase kinetic parameters $CaTD_{50}$ and $CaTD_{75-25}$. *miR-25* in contrast slowed the uptake phase parameters but did not appreciably affect V_{max} upstroke. (*n*>550 cells per group). Box defines interquartile range; whiskers = ±5th and 95th percentile; dots = outliers.

Although IP3R1 might be a direct target of *miR-25*, several lines of evidence suggest that it is unlikely to mediate *miR-25*'s effect in heart failure. IP3Rs are intracellular ligand-gated Ca^{2+} release channels[42] that in the sarcoplasmic reticulum are associated with excitation-contraction coupling or spontaneous Ca^{2+} release and enhanced Ca^{2+} transients, whereas in the nuclear envelope promote nuclear Ca^{2+} signaling[43-45], but a specific role for IP3R1 in heart failure has not been identified. Nonetheless, *miR-25* control of IP3R1 might play a critical role under conditions that sensitize cardiomyocytes to IP3, such in response to endothelin-1, angiotensin and phenylephrine[24] or in local Ca^{2+} control[25].
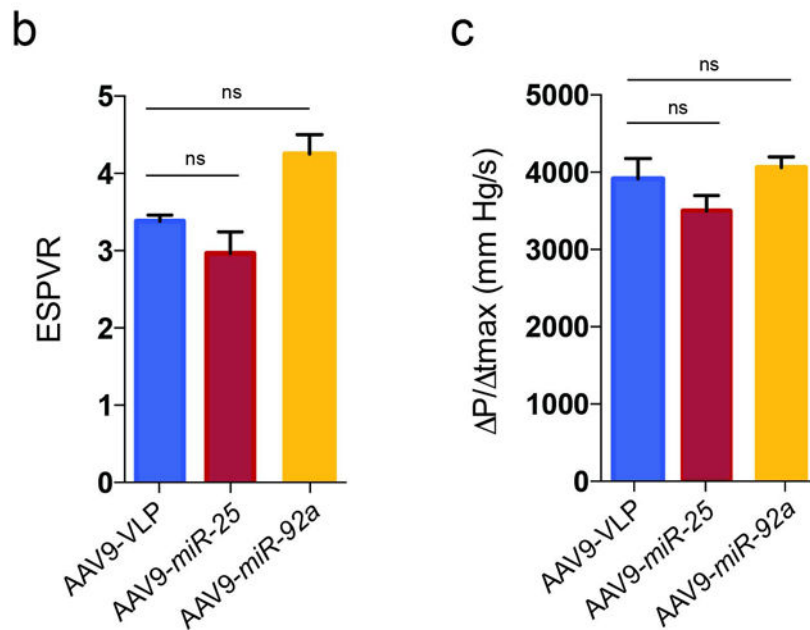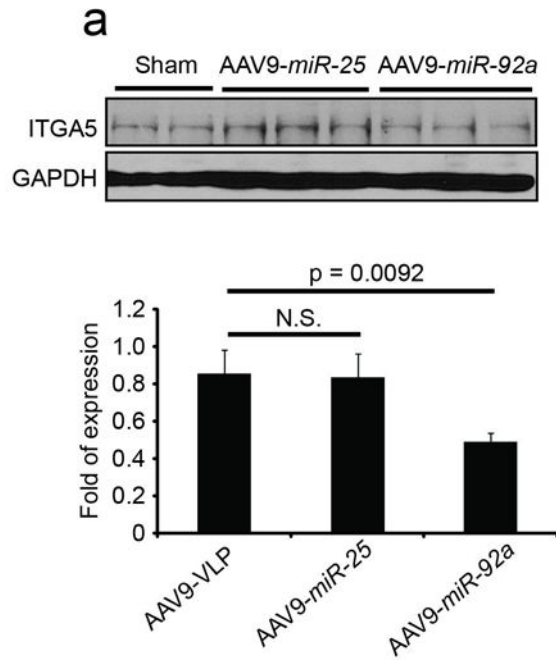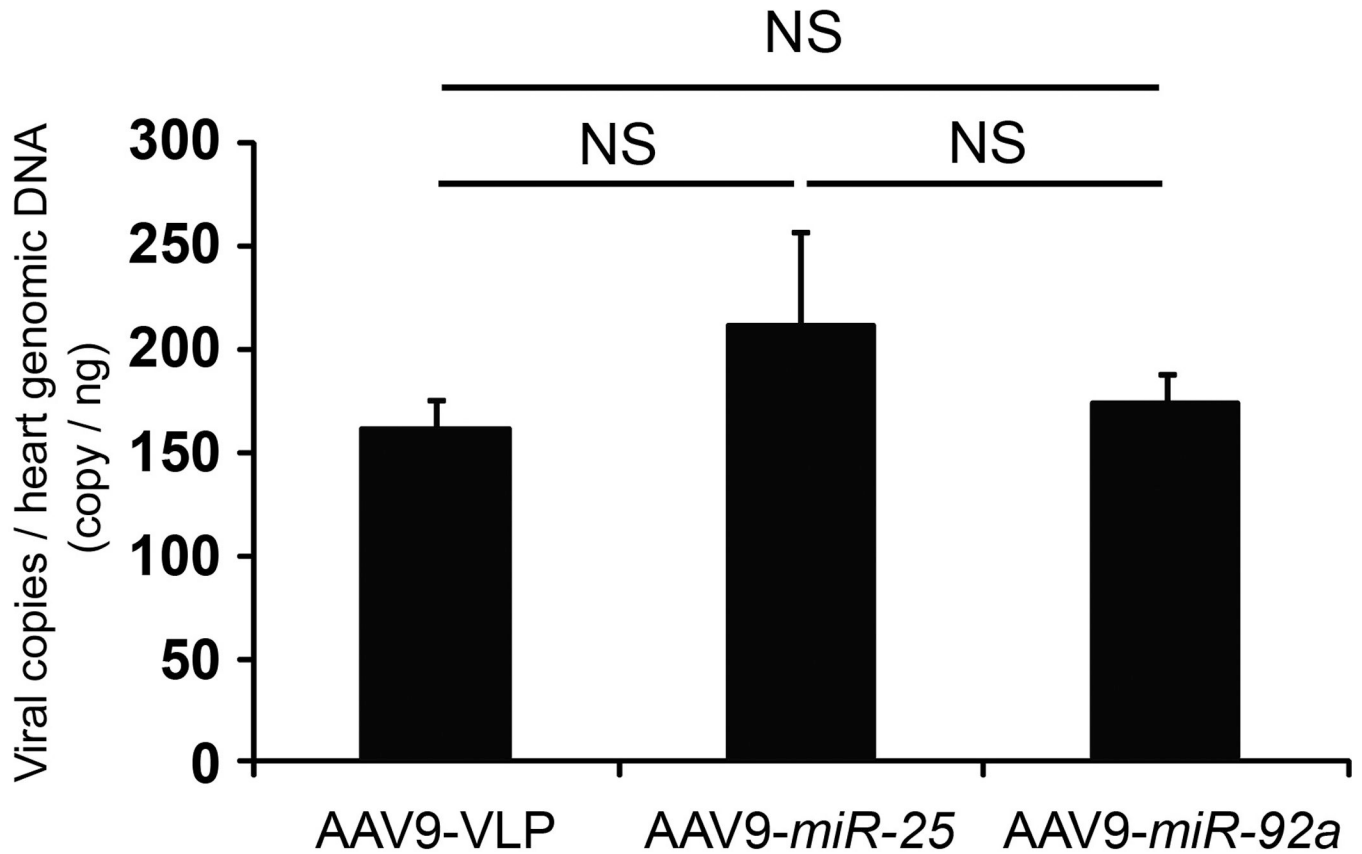
Extended Data Fig. 4. Effect of *miR-25* and *miR-92a* overexpression *in vivo*
Effect of AAV9 cardiac gene transfer of *miR-25* and *miR-92a* on target protein levels (**a**).
Cardiac gene transfer of *miR-25* and *miR-92a* increased levels of their respective
microRNAs but *miR-92a* was selective against confirmed target integrin subunit α5
(ITGA5). Effects of AAV9 cardiac gene transfer of *miR-25* and *miR-92a* on cardiac function
(**b-c**). Tendency towards decreased cardiac function in both ESPVR (**b**) and dP/dtmax (**c**) in
AAV9-*miR-25* animals relative to control (AAV9-VLP) and AAV9-*miR-92a* treated

animals. *n*=5 (AAV9-VLP); 4 (AAV9-*miR-25*); 5 (AAV9-*miR-92a*) for panels **b-c** . In all panels data is represented as mean ± s.e.m.


Extended Data Fig. 5. AAV9-mediated gene transfer integration in ventricular myocardium
The number of integrated *miR-25 and miR-92a* copies in ventricular myocardium 6 weeks after AAV gene transfer, determined by quantitative PCR (see **Detailed Methods**). *n* = 5 (AAV9-VLP), *n* = 4 (AAV9-*miR-25*) and *n* = 5 (AAV9-*miR-92a*). Data is represented as mean ± s.e.m.
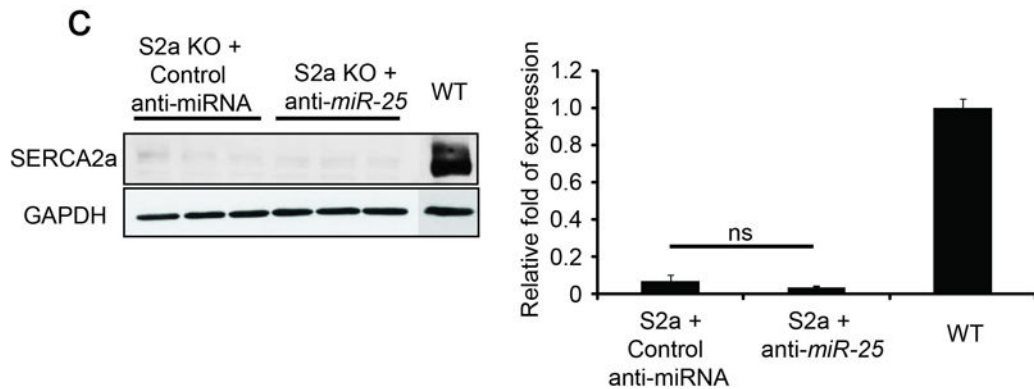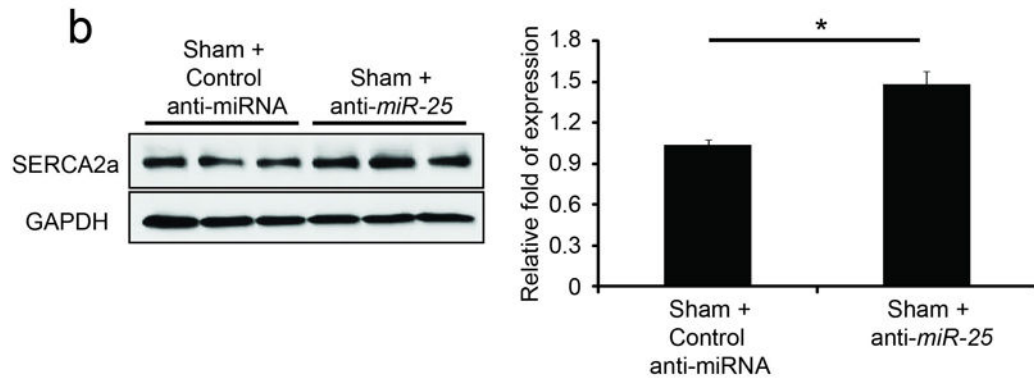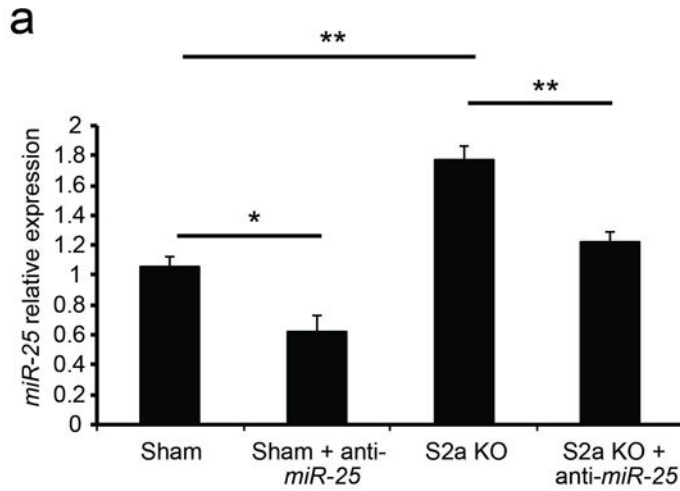
Extended Data Fig. 6. Effects of anti-*miR-25* on endogenous *miR-25* and SERCA2a in WT and *Serca2a*-null hearts

Anti-*miR-25* or control (scrambled sequence) anti-miR was administered intravenously to sham-operated WT mice (Sham) or to unoperated *Serca2a*-cardiomyocyte null (S2a KO) mice[39], as for the experiments in Fig. 4 (see **Detailed Methods**). Sham-operated animals were injected with anti-miRs 1 week after surgery and analyzed at 4 weeks. S2a KO animals were injected with 4-OH tamoxifen i.p. for 4 days to delete *Serca2a* (see **Detailed Methods**), injected with anti-miRs 1 week later and analyzed 4 weeks later (5 weeks from

initial 4-OH-tamoxifen injection). Note that anti-*miR-25* decreased endogenous *miR-25* levels in sham-operated WT and S2a KO mice relative to control-treated animals (*n* = 3) (**a**). Furthermore, SERCA2a protein levels increased in the anti-*miR-25* treated WT animals relative to control (*n* = 3) (**b**). SERCA2a is absent in S2a KO hearts (**c**). In all panels data is represented as mean ± s.e.m.
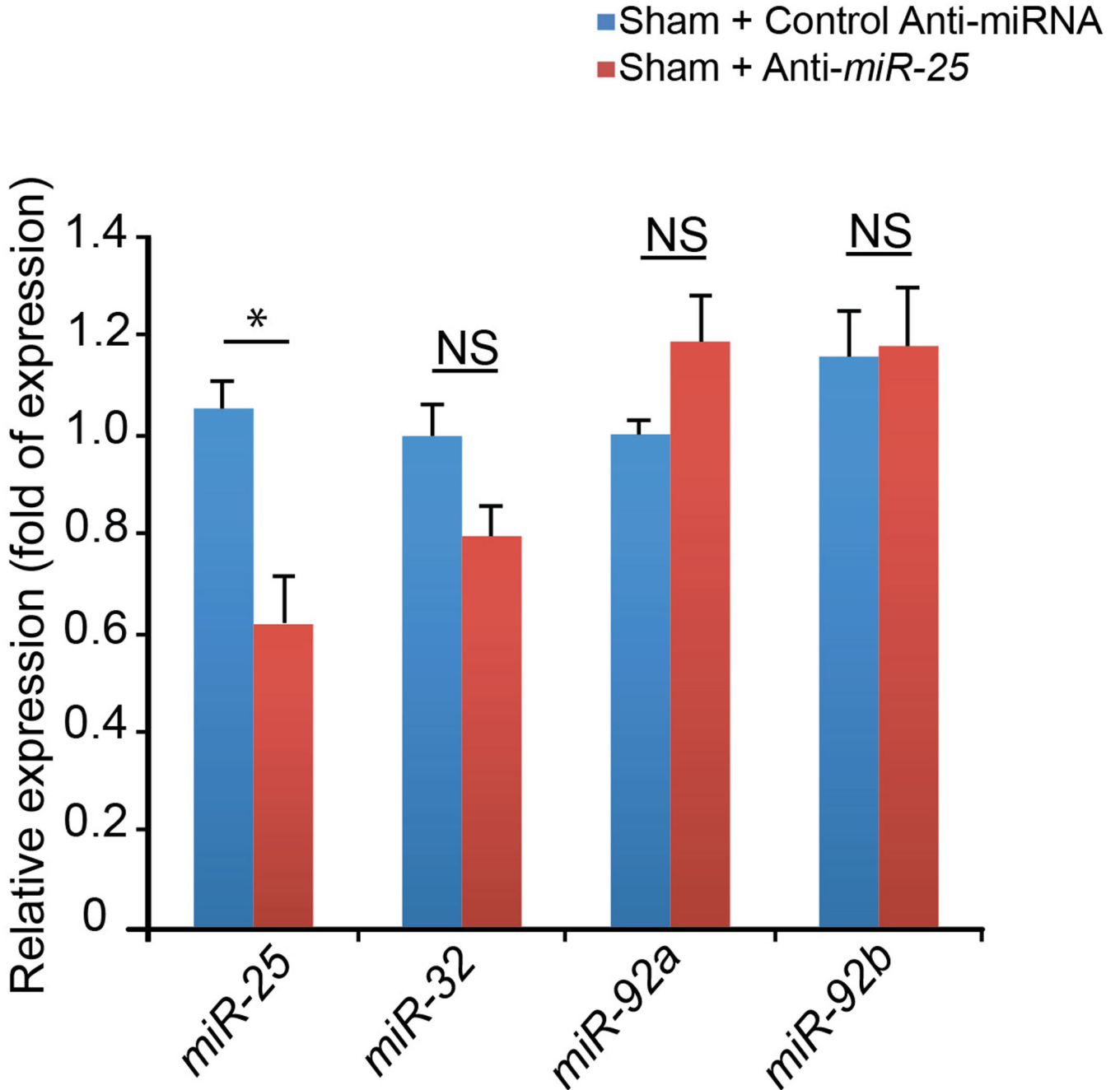
Extended Data Fig. 7. Selectivity of anti-*miR-25* on *miR-25* family
Expression levels of *miR-25* and family members (*miR-32*, *miR-92a*, and *miR-92b*) in sham-operated mice that had been injected with anti-*miR-25* or control (scrambled sequence) anti-

miR as in Fig. 4 (see **Detailed Methods**) ($n = 3$). Note that control anti-miR in sham-operated animals did not alter expression of any of the miRs tested (blue bars). In contrast, anti-*miR-25* significantly reduced levels of *miR-25* but not other family members in sham-operated animals (red bars). Data is represented as mean ± s.e.m.

a

Sham + control anti-miR   Sham + anti-*miR-25*   S2a KO + control anti-miR   S2a KO + anti-*miR-25*
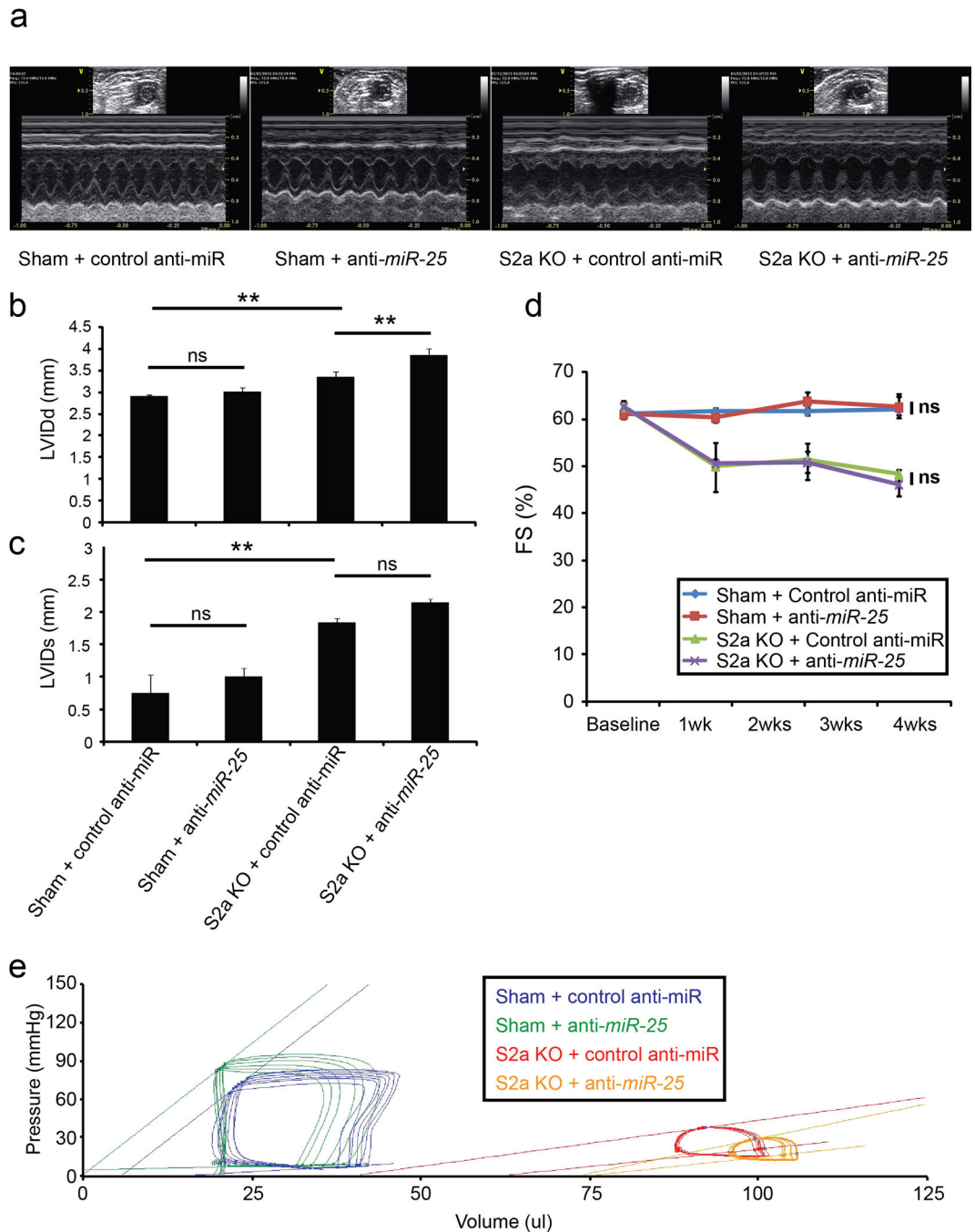
Extended Data Fig. 8. Effects of anti-*miR-25* on cardiac function of WT and *Serca2a*-null hearts
Anti-*miR-25* or control (scrambled sequence) anti-miR was administered intravenously to sham-operated WT mice (Sham) or to unoperated Serca2a-cardiomyocyte null (S2a KO)

mice[39], as for the experiments in Fig. 4 (see **Detailed Methods**). Sham-operated animals were injected with anti-miRs 1 week after surgery and followed by echocardiography. S2a KO animals were generated by injection with 4-OH tamoxifen i.p. for 4 days (see **Detailed Methods**) to delete *Serca2a*, then injected with anti-miRs 1 week later and followed by echocardiography.

Representative two-dimensional guided M-mode images of the left ventricles from WT and S2a KO mice (**a**). Echocardiographic indices of left ventricular inner dimension during diastole, LVIDd (**b**) and systole, LVIDs (**c**) (n = 3 (sham+control); 8, (sham+anti-*miR-25*); 7 (S2a KO+control); 11 (S2a-KO+anti-*miR-25*) 4 weeks after control or anti-miR injection. Echocardiographic measurement of fractional shortening (FS) expressed as a percentage at time points after control or anti-miR injection (n = 4 (sham+control); 3 (sham+anti-*miR-25*); 3 (S2a KO+control); 3 (S2a KO+anti-*miR-25*)) (**d**). S2a KO mice show characteristic dilation and decline in cardiac function following 4-OH tamoxifen-induced excision of *Serca2a*[40]; ***, $P < 0.001$ (Student's t-test for difference between S2a KO and Sham-operated control anti-miR groups at week 4 following injection).

Hemodynamic effect of anti-*miR-25* and control anti-miR injection represented by pressure-volume plots of treatment cohorts as indicated 4 weeks after injection of control or anti-miR (**e**). Note that specific anti-*miR-25* and control anti-miR acted similarly in sham-operated WT animals (n = 3 (sham+control); 3, (sham+anti-miR-25); 2 (S2a KO+control); 3 (S2a-KO +anti-miR-25). Moreover, anti-*miR-25* did not increase cardiac function of S2a KO mice, unlike TAC-operated WT mice (Fig. 4), suggesting that the beneficial effect on cardiac function depends on SERCA2a. In all panels data is represented as mean ± s.e.m.
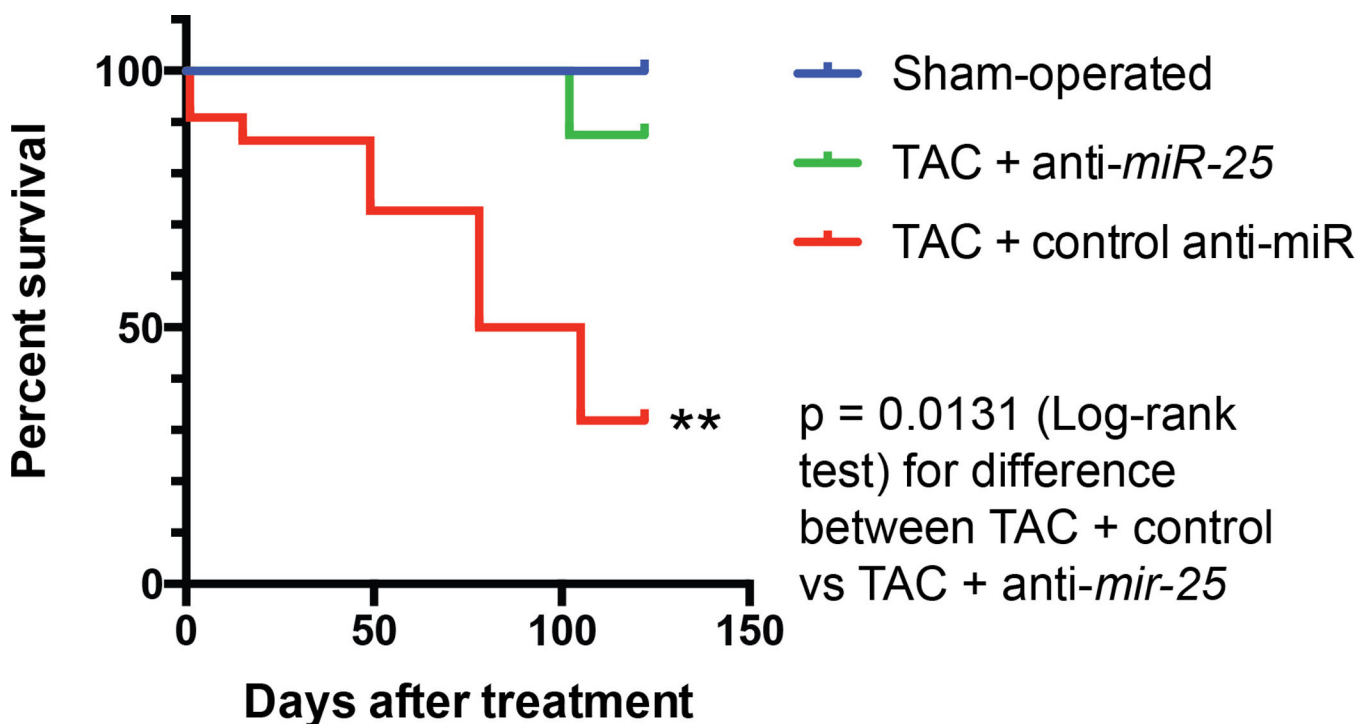
Extended Data Fig. 9. Kaplan Meier survival curve for anti-*miR-25* treatment

Survival probability is plotted over time, showing cumulative protective effect of anti-*miR-25* relative to control (scrambled sequence) anti-miR injections following trans-aortic constriction (TAC). The summary of two experiments is shown plotting time from injection. Groups were sham-operated ($n = 8$), TAC + anti-*miR-25* ($n = 8$), TAC + control (scrambled sequence) anti-miR ($n = 22$). Note that injection with specific anti-*miR-25* increased survival ($P = 0.0131$, Log-rank test) relative to TAC + control miR.
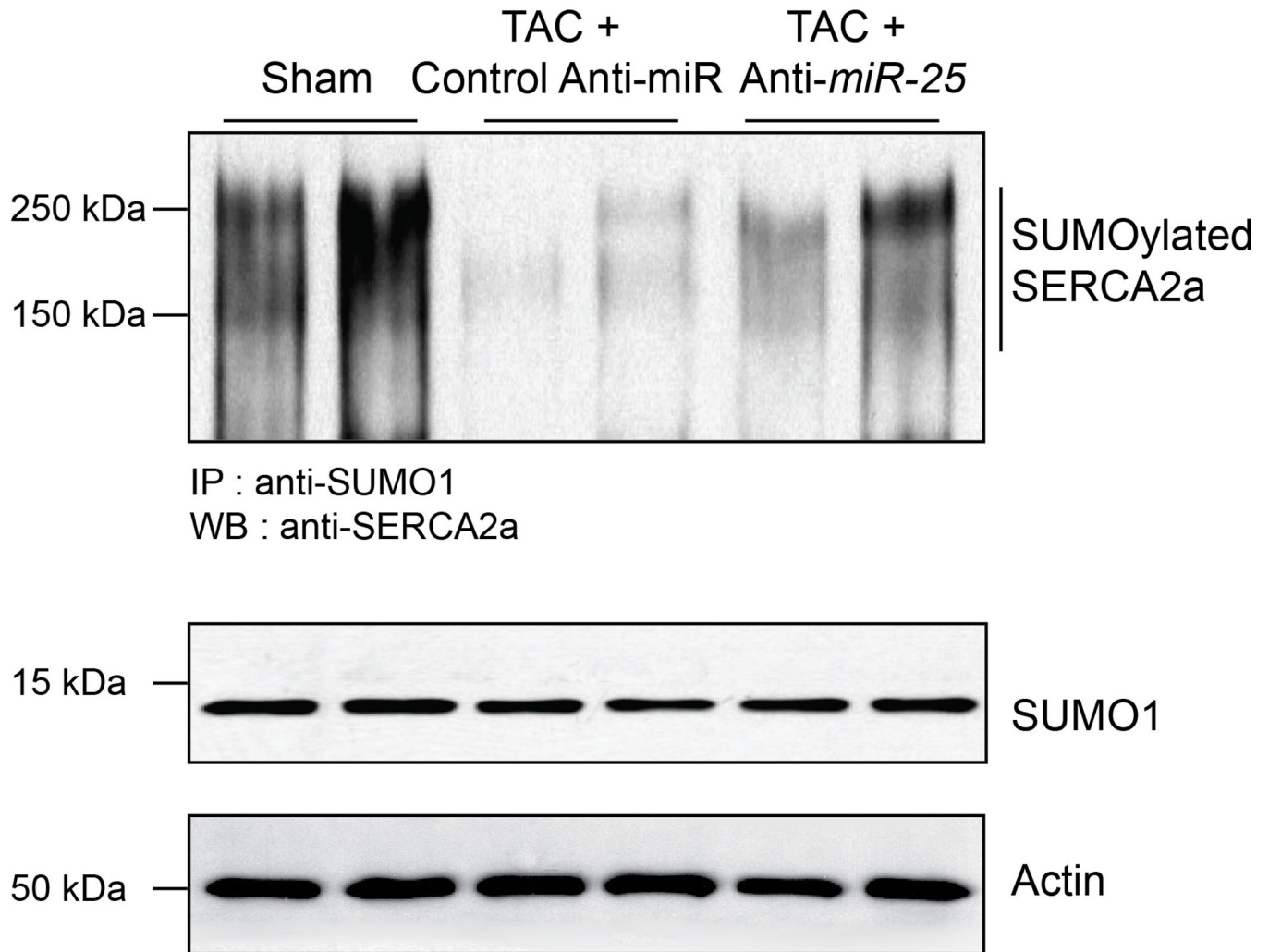
Extended Data Fig. 10. Effect of anti-*miR-25* on accumulation of SUMOylated SERCA2a

Immunoblots of lysates from heart tissue at termination of the *in vivo* study of Fig. 4 (5.5 months post-TAC, corresponding to 3.5 months post-injection of anti-*miR-25* or control (scrambled sequence) anti-miR). Lysates were immunoprecipitated with anti-SUMO1 followed by Western blotting with anti-SERCA2a, as in[22]. Note reduction in SUMOylated SERCA2a upon TAC in the control anti-miR treated hearts, but restoration of expression following specific anti-*miR-25* injection. Total levels of SUMO1 and actin are shown.

Author Manuscript

Author Manuscript

Author Manuscript

Author Manuscript

Supplementary Material

Refer to Web version on PubMed Central for supplementary material.

Acknowledgements

References

1. Bonow, RO.; Mann, DL.; Zipes, DP.; Libby, P. Braunwald's Heart Disease. Saunders; 2011.

2. Meyer M, et al. Alterations of sarcoplasmic reticulum proteins in failing human dilated cardiomyopathy. Circulation. 1995; 92:778–784. [PubMed: 7641356]

3. Jessup M, et al. Calcium Upregulation by Percutaneous Administration of Gene Therapy in Cardiac Disease (CUPID): a phase 2 trial of intracoronary gene therapy of sarcoplasmic reticulum Ca2+-ATPase in patients with advanced heart failure. Circulation. 2011; 124:304–313. [PubMed: 21709064]

4. Ikeda S, et al. Altered microRNA expression in human heart disease. Physiological genomics. 2007; 31:367–373. [PubMed: 17712037]

5. Leptidis S, et al. A deep sequencing approach to uncover the miRNOME in the human heart. PLoS ONE. 2013; 8:e57800. [PubMed: 23460909]

6. Shah AM, Mann DL. In search of new therapeutic targets and strategies for heart failure: recent advances in basic science. The Lancet. 2011; 378:704–712.

7. Mudd JO, Kass DA. Tackling heart failure in the twenty-first century. Nature. 2008; 451:919–928. [PubMed: 18288181]

8. Greenstein JL, Winslow RL. Integrative systems models of cardiac excitation-contraction coupling. Circulation research. 2011; 108:70–84. [PubMed: 21212390]

9. Bartel DP. MicroRNAs: target recognition and regulatory functions. Cell. 2009; 136:215–233. [PubMed: 19167326]

10. Filipowicz W, Bhattacharyya SN, Sonenberg N. Mechanisms of post-transcriptional regulation by microRNAs: are the answers in sight? Nature reviews. Genetics. 2008; 9:102–114.

11. Gurha P, et al. Targeted deletion of microRNA-22 promotes stress-induced cardiac dilation and contractile dysfunction. Circulation. 2012; 125:2751–2761. [PubMed: 22570371]

12. Kawase Y, et al. Reversal of cardiac dysfunction after long-term expression of SERCA2a by gene transfer in a pre-clinical model of heart failure. Journal of the American College of Cardiology. 2008; 51:1112–1119. [PubMed: 18342232]

13. Jessup M, et al. Calcium Upregulation by Percutaneous Administration of Gene Therapy in Cardiac Disease (CUPID): A Phase 2 Trial of Intracoronary Gene Therapy of Sarcoplasmic Reticulum Ca2+-ATPase in Patients With Advanced Heart Failure. Circulation. 2011

14. Shirdel EA, Xie W, Mak TW, Jurisica I. NAViGaTing the micronome--using multiple microRNA prediction databases to identify signalling pathway-associated microRNAs. PLoS ONE. 2011; 6:e17429. [PubMed: 21364759]

15. Lemons D, Maurya MR, Subramaniam S, Mercola M. Developing microRNA screening as a functional genomics tool for disease research. Front Physiol. 2013; 4:223. [PubMed: 23986717]

16. Cerignoli F, et al. High throughput measurement of Ca(2+) dynamics for drug risk assessment in human stem cell-derived cardiomyocytes by kinetic image cytometry. Journal of pharmacological and toxicological methods. 2012; 66:246–256. [PubMed: 22926323]

17. Beuckelmann DJ, Nabauer M, Erdmann E. Intracellular calcium handling in isolated ventricular myocytes from patients with terminal heart failure. Circulation. 1992; 85:1046–1055. [PubMed: 1311223]

18. Piacentino V 3rd, et al. Cellular basis of abnormal calcium transients of failing human ventricular myocytes. Circulation research. 2003; 92:651–658. [PubMed: 12600875]

19. Krutzfeldt J, et al. Silencing of microRNAs in vivo with 'antagomirs'. Nature. 2005; 438:685–689. [PubMed: 16258535]

20. Bonauer A, et al. MicroRNA-92a controls angiogenesis and functional recovery of ischemic tissues in mice. Science (New York, N.Y. 2009; 324:1710–1713.

21. Helwak A, Kudla G, Dudnakova T, Tollervey D. Mapping the human miRNA interactome by CLASH reveals frequent noncanonical binding. Cell. 2013; 153:654–665. [PubMed: 23622248]

22. Kho C, et al. SUMO1-dependent modulation of SERCA2a in heart failure. Nature. 2011; 477:601–605. [PubMed: 21900893]

23. Kho C, Lee A, Hajjar RJ. Altered sarcoplasmic reticulum calcium cycling--targets for heart failure therapy. Nature reviews. Cardiology. 2012; 9:717–733. [PubMed: 23090087]

24. Higazi DR, et al. Endothelin-1-stimulated InsP3-induced Ca2+ release is a nexus for hypertrophic signaling in cardiac myocytes. Molecular Cell. 2009; 33:472–482. [PubMed: 19250908]

25. Hulot JS, et al. Critical role for stromal interaction molecule 1 in cardiac hypertrophy. Circulation. 2011; 124:796–805. [PubMed: 21810664]

26. Fu Y, et al. Regulation of NADPH oxidase activity is associated with miRNA-25-mediated NOX4 expression in experimental diabetic nephropathy. Am J Nephrol. 2010; 32:581–589. [PubMed: 21071935]

27. Schmidt HH, Wingler K, Kleinschnitz C, Dusting G. NOX4 is a Janus-faced reactive oxygen species generating NADPH oxidase. Circulation research. 2012; 111:e15–e16. author reply e17-18. [PubMed: 22723224]

28. Dirkx E, et al. Nfat and miR-25 cooperate to reactivate the transcription factor Hand2 in heart failure. Nature cell biology. 2013; 15:1282–1293. [PubMed: 24161931]

References (for Online Methods and Extended Data)

29. Colas AR, et al. Whole-genome microRNA screening identifies let-7 and mir-18 as regulators of germ layer formation during early embryogenesis. Genes & development. 2012; 26:2567–2579. [PubMed: 23152446]

30. McKeithan W, Colas A, Bushway PJ, Ray S, Mercola M. Serum-Free Generation of Multipotent Mesoderm (Kdr-positive) Progenitor Cells in Mouse Embryonic Stem Cells For Functional Genomics Screening. Current Protocols. 2012 in press.

31. Roy S, et al. MicroRNA expression in response to murine myocardial infarction: miR-21 regulates fibroblast metalloprotease-2 via phosphatase and tensin homologue. Cardiovascular research. 2009; 82:21–29. [PubMed: 19147652]

32. Matkovich SJ, et al. Reciprocal regulation of myocardial microRNAs and messenger RNA in human cardiomyopathy and reversal of the microRNA signature by biomechanical support. Circulation. 2009; 119:1263–1271. [PubMed: 19237659]

33. van Rooij E, et al. Dysregulation of microRNAs after myocardial infarction reveals a role of miR-29 in cardiac fibrosis. Proceedings of the National Academy of Sciences of the United States of America. 2008; 105:13027–13032. [PubMed: 18723672]

34. Cheng Y, et al. MicroRNAs are aberrantly expressed in hypertrophic heart: do they play a role in cardiac hypertrophy? The American journal of pathology. 2007; 170:1831–1840. [PubMed: 17525252]

35. Tatsuguchi M, et al. Expression of microRNAs is dynamically regulated during cardiomyocyte hypertrophy. Journal of Molecular and Cellular Cardiology. 2007; 42:1137–1141. [PubMed: 17498736]

36. Sayed D, Hong C, Chen IY, Lypowy J, Abdellatif M. MicroRNAs play an essential role in the development of cardiac hypertrophy. Circulation research. 2007; 100:416–424. [PubMed: 17234972]

37. van Rooij E, et al. A signature pattern of stress-responsive microRNAs that can evoke cardiac hypertrophy and heart failure. Proceedings of the National Academy of Sciences of the United States of America. 2006; 103:18255–18260. [PubMed: 17108080]

38. Zolotukhin S, et al. Recombinant adeno-associated virus purification using novel methods improves infectious titer and yield. Gene therapy. 1999; 6:973–985. [PubMed: 10455399]

39. Andersson KB, et al. Moderate heart dysfunction in mice with inducible cardiomyocyte-specific excision of the Serca2 gene. Journal of Molecular and Cellular Cardiology. 2009; 47:180–187. [PubMed: 19328205]

40. Swift F, et al. Extreme sarcoplasmic reticulum volume loss and compensatory T-tubule remodeling after Serca2 knockout. Proceedings of the National Academy of Sciences of the United States of America. 2012; 109:3997–4001. [PubMed: 22355118]

41. Pacher P, Nagayama T, Mukhopadhyay P, Batkai S, Kass DA. Measurement of cardiac function using pressure–volume conductance catheter technique in mice and rats. Nature protocols. 2008; 3:1422–1434. [PubMed: 18772869]

42. Bers DM. Calcium cycling and signaling in cardiac myocytes. Annual Review of Physiology. 2008; 70:23–49.

43. Kockskamper J, et al. Emerging roles of inositol 1,4,5-trisphosphate signaling in cardiac myocytes. Journal of Molecular and Cellular Cardiology. 2008; 45:128–147. [PubMed: 18603259]

44. Bootman MD, Roderick HL. Why, where, and when do cardiac myocytes express inositol 1,4,5-trisphosphate receptors? American journal of physiology. Heart and circulatory physiology. 2008; 294:H579–H581. [PubMed: 18065525]

45. Zima AV, Bare DJ, Mignery GA, Blatter LA. IP3-dependent nuclear Ca2+ signalling in the mammalian heart. The Journal of physiology. 2007; 584:601–611. [PubMed: 17761776]

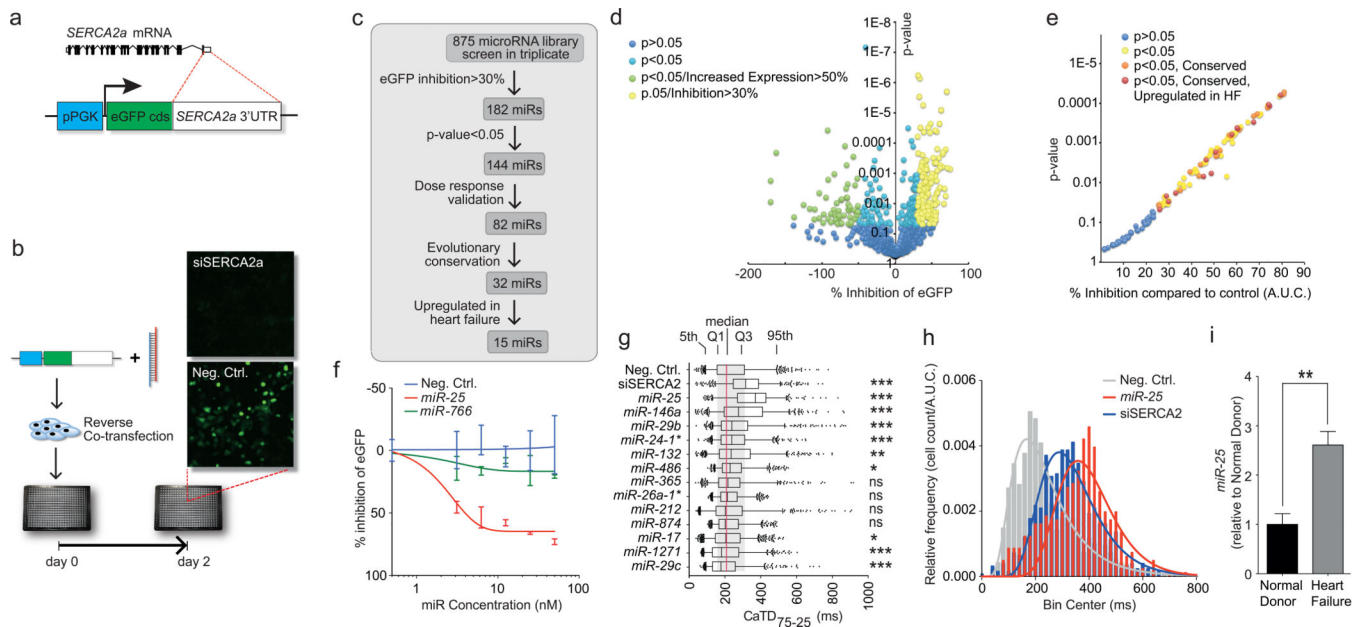**Figure 1. High content screening identifies miRs that control SERCA2a**

a,b. Target sensor construct (**a**) and screening workflow (**b**).

c. Screening summary.

d,e. Primary (**d**) and confirmatory (**e**) screen data plotted as % inhibition relative to siRNA against *Serca2a* (100% inhibition) and scrambled sequence control (0% inhibition) (X-axis) and *P*-value from Student's t-test (Y-axis).

f. eGFP-SERCA2a inhibition by *miR-25* and inactive *miR-766* relative to scrambled sequence control $n = 10$.

g. Ca^{2+} transient kinetic analysis of HL-1 cells transfected with miRs that inhibited eGFP-SERCA2a (panel **e**) and are evolutionarily conserved and upregulated in human heart failure. CaTD$_{75-25}$ is decay phase duration from 75% to 25% maximal value ($n > 550$ cells per group). Box = 25th to 75th percentiles; whiskers = 5th and 95th percentiles; dots = outliers. *, **, *** = $P < 0.05$, < 0.01, < 0.001. ns = not significant (one-tailed ANOVA).

h. Frequency distribution and log-normal curve fits for CaTD$_{75-25}$ values from panel **f**, normalized to sample size. Both siSERCA2a and *miR-25* increased CaTD$_{75-25}$ values.

i. *miR-25* is upregulated in human heart failure samples, by Q-PCR. Error bars = s.e.m. ** indicates $P < 0.01$ ($n = 5$), Student's t-test. All replicates (n) are biological.
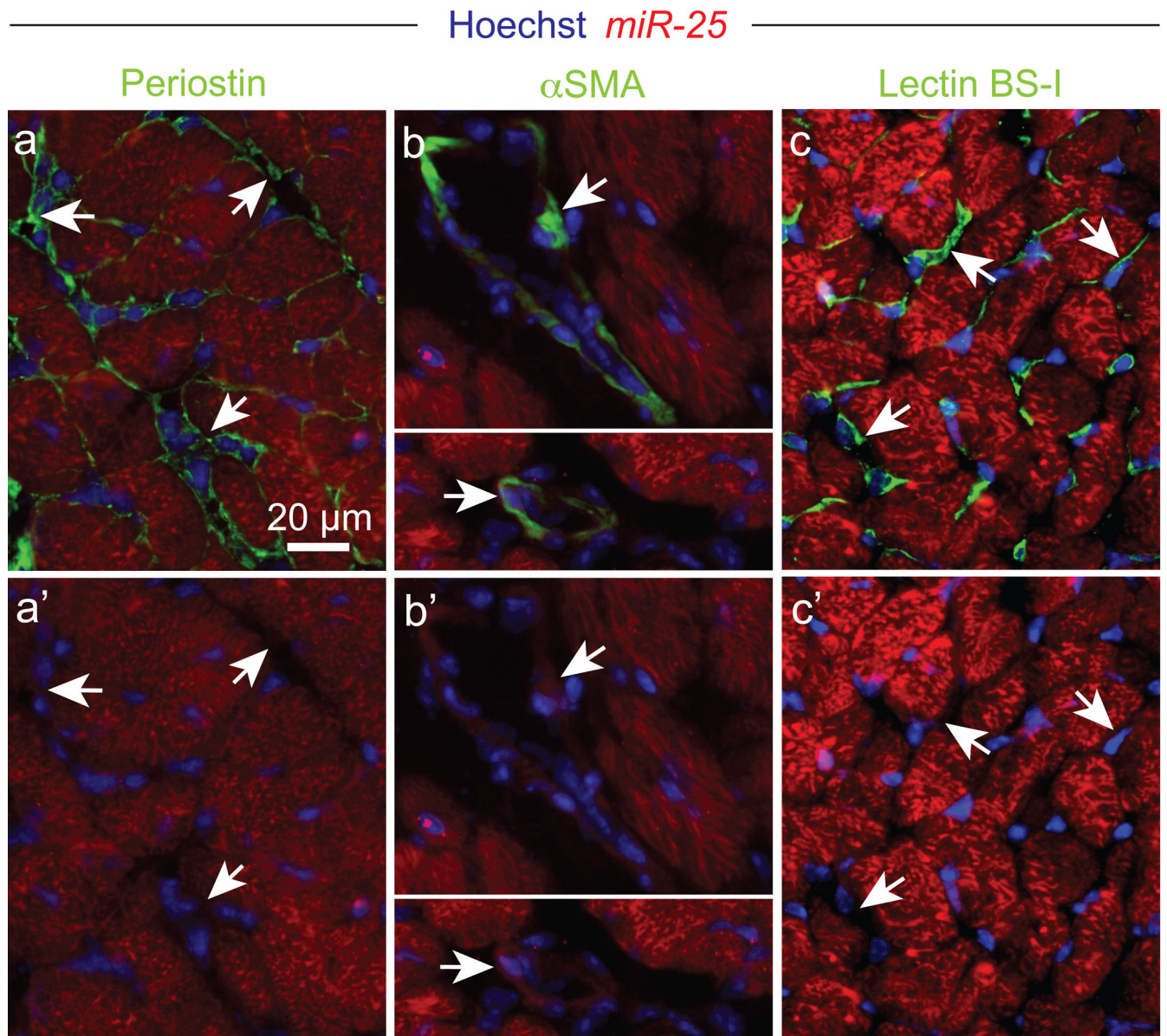
Figure 2. Endogenous *miR-25* expression in the heart
In situ hybridization revealing endogenous *miR-25* expression in failing left ventricular myocardium (red) compared to periostin (**a,a'**), αSMA (**b,b'**) and lectin BS-1 (**c,c'**) staining (each in green). Hoechst 33342 staining marks nuclei (blue). Arrows indicate examples of non-cardiomyocytes. Scale bar equals 20 μm. Data are representative of 2 biological replicates.
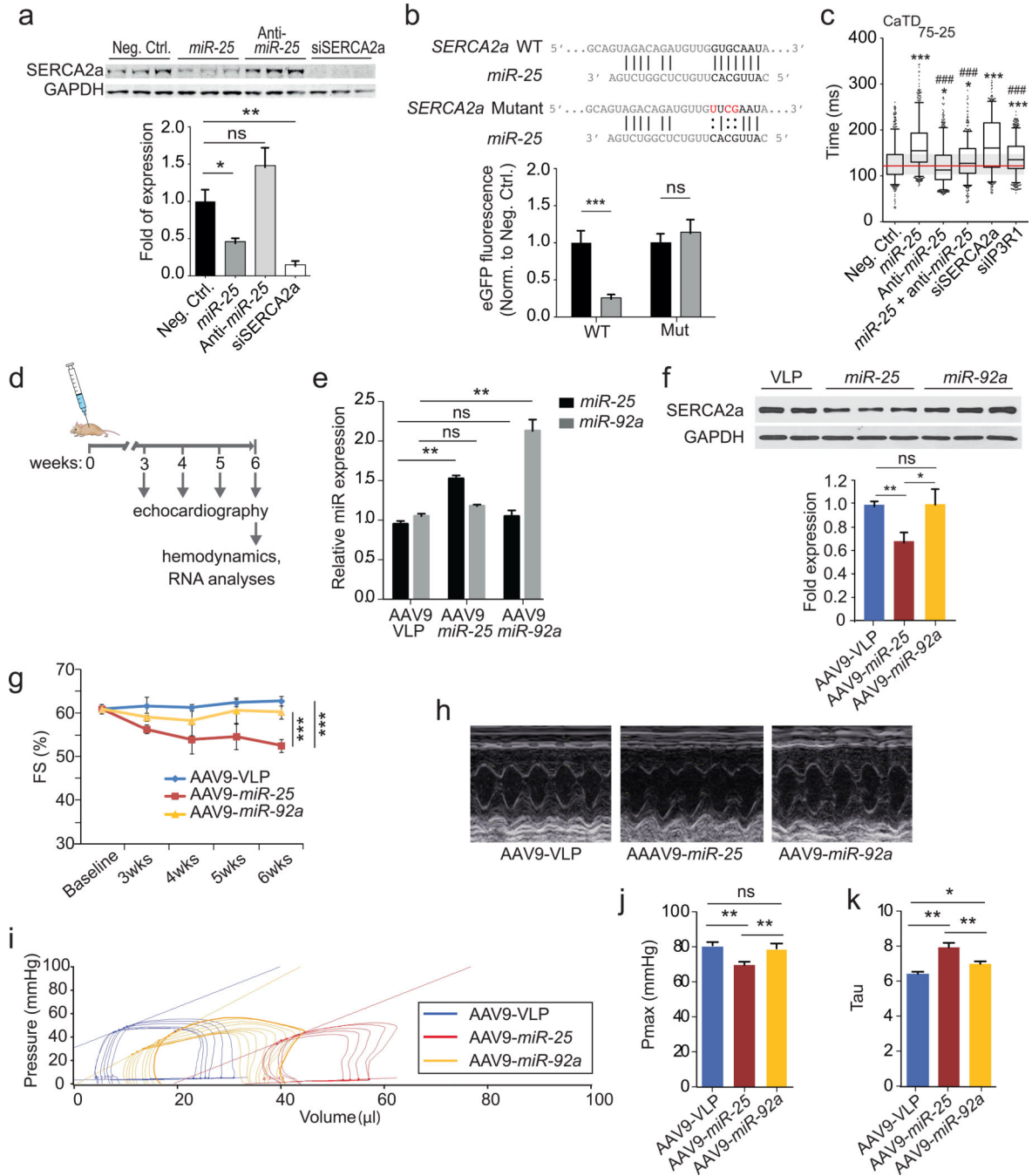
Figure 3. *miR-25* directly targets SERCA2a and regulates contractile Ca^{2+} kinetics

a. Effects of *miR-25*, anti-*miR-25* and controls (scrambled sequence and SERCA2a siRNA) on SERCA2a protein levels.

b. Mutagenesis of the putative *mir-25* recognition element in the SERCA2a mRNA 3'UTR abolished inhibition by *miR-25*. *, ** indicate $P < 0.05$ and 0.01 ($n = 10$) (Student's t-test), compared to control.

c. Anti-*miR-25* diminished the effect of *miR-25* on CaTD$_{75-25}$ in transfected HL-1 cells. siRNA to IP3R1 had a minimal effect. Extended Data Fig. 3 shows additional parameters

and similar results using NRVCs. Box plots as in Fig. 1g. *,# indicate significant difference (* or # = $P < 0.05$, ** or ## = $P < 0.01$, *** or ### = $P < 0.001$, one-tailed ANOVA) from negative control (*) or *miR-25* (#) ($n > 550$ cells per group).

d. Protocol for AAV9 cardiac gene transfer.

e. AAV-*miR-25* ($n = 4$) and AAV-*miR-92a* ($n = 5$) increased levels of their respective microRNAs relative to AAV-VLP control ($n = 3$).

f–h. miR-25, but not *miR-92a* diminished SERCA2a protein levels (**f**) and fractional shortening (FS; percentage) following injection ($n = 5$ for each cohort; **g**). LV M-mode images (**h**).

I–k. Pronounced effect of *miR-25* on pressure-volume relationship (**i**) and P_{max} (**j**) showing decreased function relative to *miR-92a* and control AAV9; and the effect on Tau, the time constant for LV relaxation, suggestive of diastolic dysfunction ($n = 5$, AAV9-VLP; $n = 4$, AAV9-*miR-25*; $n = 5$, AAV9-*miR-92a*).

Data are represented as mean ± s.e.m in all panels except c. All replicates (n) are biological.
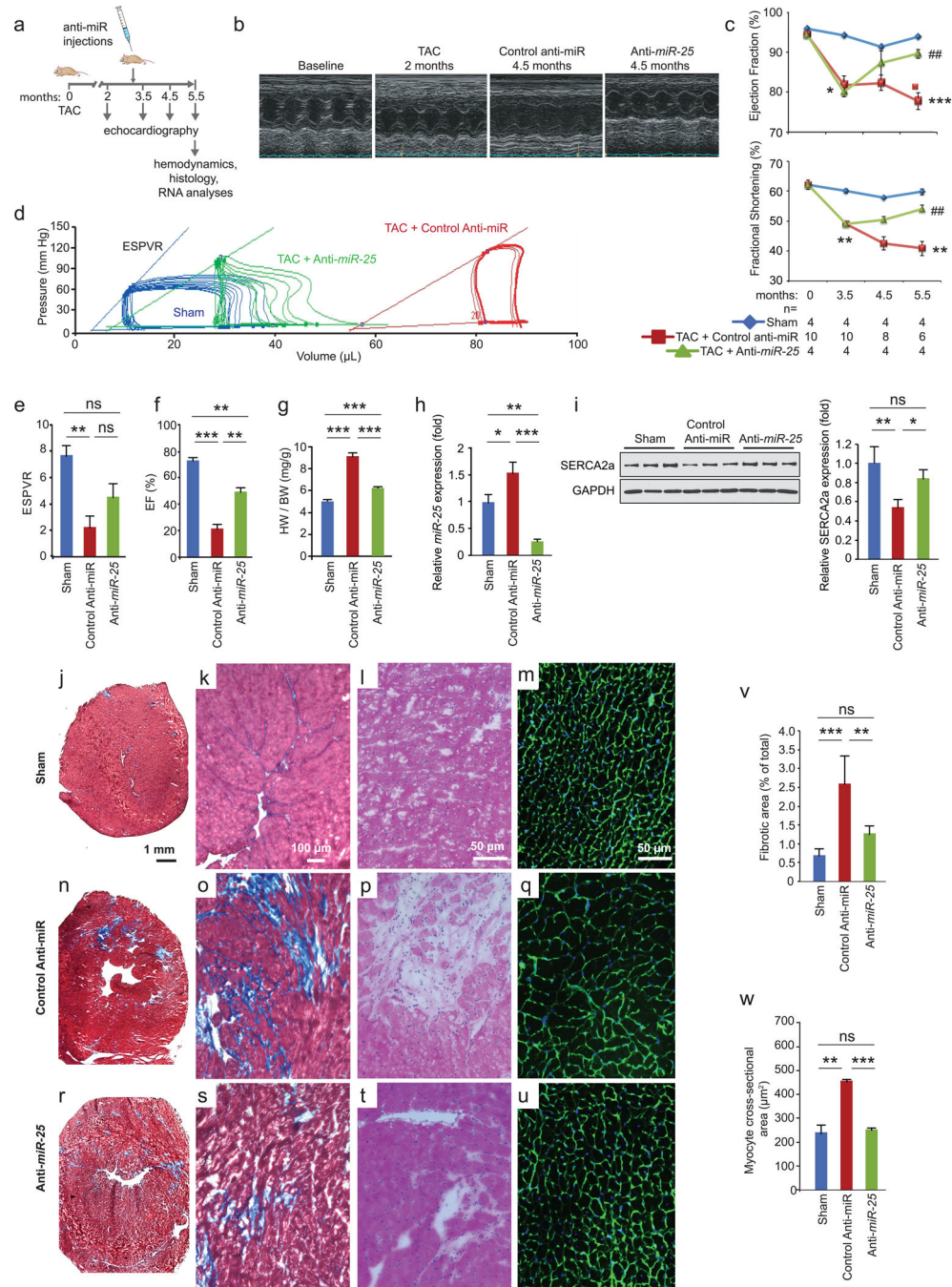
Figure 4. Inhibition of *miR-25* normalizes TAC-induced cardiac dysfunction

a. Protocol for anti-*miR-25* therapy in the mouse TAC heart failure model.

b. LV M-mode images showing dilation with control anti-miR in contrast to anti-*miR-25* injected mice.

c. Effect on echocardiographic indices of left ventricular function: ejection fraction (EF) and fractional shortening (FS) expressed as percentages. The number of animals initiated is $n = 4$ (sham operated), 10 (TAC + control anti-miR), and 4 (TAC + anti-*miR-25*); the numbers

analyzed per time point are indicated and reflect deaths in the TAC + control anti-miR group.

d–f. Hemodynamic effects. Pressure-volume plots of treatment cohorts as indicated (**d**). Note anti-*miR-25* trend towards normalization of hemodynamic indices of end systolic pressure volume relationship (ESPVR, slope of lines in **d**) (**e**), and EF (**f**). $n = 4$ (sham operated), 4 (TAC + control anti-miR), and 3 (TAC + anti-*miR-25*).

g. Heart weight to body weight ratio. $n = 5$ (sham), 8 (TAC + control anti-miR), and 4 (TAC + anti-*miR-25*).

h,i. Effect of treatment on endogenous *miR-25* levels (**h**, Q-PCR, $n = 4$) and SERCA2a protein (**I**, immunoblotting, $n = 3$).

j–w. Masson's trichrome (**j,k,n,o,r,s**), hematoxylin/eosin (**l,p,t**), and wheat germ agglutinin (WGA) (**m,q,u**) stained sections of hearts and LV wall. Quantified fibrotic area (**v**) [$n = 3$ (sham operated), 4 (TAC + control anti-miR), and 5 (TAC + anti-*miR-25*]. Average cardiomyocyte cross sectional area (**w**) ($n = 3$ for all cohorts).

For all panels, mean ± s.e.m. *, # indicate significant difference (* or #, ** or ##, *** or ### = P <0.05, <0.01, <0.001) (Student's t-test) between sham and control-anti-miR (*) or control anti-miR and anti-*miR-25* (#). All replicates (n) are biological.